AD-A087 557 UNITED TECHNOLOGIES RESEARCH CENTER EAST HARTFORD CONN F/G 7/4
CARS CONCENTRATION SENSITIVITY WITH AND WITHOUT NONRESONANT BAC--ETC(U)
JUN 80 A C ECKBRETH, R J HALL N00014-79-C-0351
UNCLASSIFIED UTRC-R80-954628-1 NL

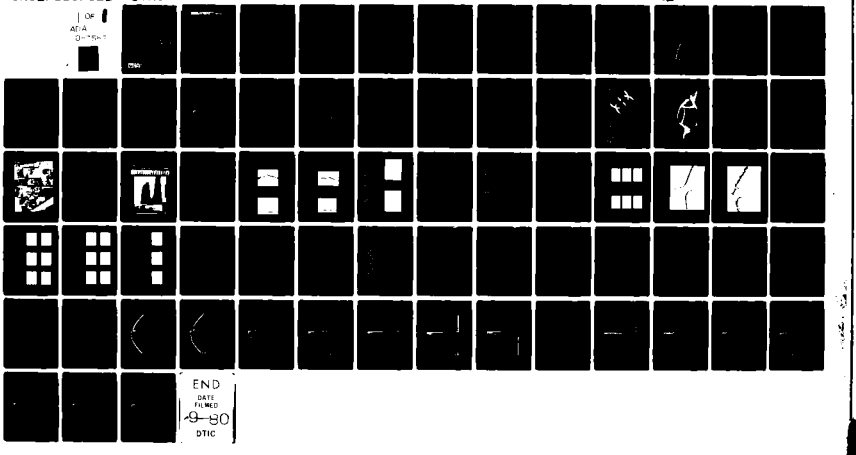

END
DATE FILMED
9-80
DTIC

R80-954628-1

LEVEL II

12 SC

CARS Concentration Sensitivity with and without Nonresonant Background Suppression

by

Alan C. Eckbreth and Robert J. Hall

Final Technical Report

June 1980

Research performed under Contract N00014-79-C-0351
for the Office of Naval Research

UNITED TECHNOLOGIES RESEARCH CENTER

UNITED TECHNOLOGIES RESEARCH CENTER

East Hartford, Connecticut 06108

(12) 70 L

(14) UTRC-R80-954628-1

(6) CARS Concentration Sensitivity with and without Nonresonant Background Suppression

by

(10) Alan C. Eckbreth and Robert J. Hall
United Techologies Research Center
East Hartford, Connecticut 06108

(9) Final Technical Report. 9 May 79-23 Apr 80,

(11) Jun 80

June 1980

(15) Research performed under Contract N00014-79-C-0351
for the Office of Naval Research

41252

Unclassified

SECURITY CLASSIFICATION OF THIS PAGE *(When Data Entered)*

REPORT DOCUMENTATION PAGE		READ INSTRUCTIONS BEFORE COMPLETING FORM
1. REPORT NUMBER R80-954628-1	2. GOVT ACCESSION NO. AD-A087557	3. RECIPIENT'S CATALOG NUMBER
4. TITLE *(and Subtitle)* CARS Concentration Sensitivity with and without Nonresonant Background Suppression		5. TYPE OF REPORT & PERIOD COVERED Final Technicial Report 5/9/79 to 4/22/80
		6. PERFORMING ORG. REPORT NUMBER R80-954628-1
7. AUTHOR(s) Alan C. Eckbreth and Robert J. Hall		8. CONTRACT OR GRANT NUMBER(s) N00014-79-C-0351
9. PERFORMING ORGANIZATION NAME AND ADDRESS United Technologies Research Center East Hartford, Connecticut 06108		10. PROGRAM ELEMENT, PROJECT, TASK AREA & WORK UNIT NUMBERS
11. CONTROLLING OFFICE NAME AND ADDRESS Office of Naval Research Dept. of the Navy 800 N. Quincy Street, Arlington, VA. 22217		12. REPORT DATE June 1980 13. NUMBER OF PAGES
14. MONITORING AGENCY NAME & ADDRESS*(if different from Controlling Office)*		15. SECURITY CLASS. *(of this report)* Unclassified 15a. DECLASSIFICATION DOWNGRADING SCHEDULE
16. DISTRIBUTION STATEMENT *(of this Report)* Unlimited		
17. DISTRIBUTION STATEMENT *(of the abstract entered in Block 20, if different from Report)*		
18. SUPPLEMENTARY NOTES		
19. KEY WORDS *(Continue on reverse side if necessary and identify by block number)* CARS, Coherent Anti-Stokes Raman Spectroscopy, Remote Combustion Diagnostics CARS Concentration Sensitivity, Polarization Sensitive CARS, Background Nonresonant Susceptibility Suppression		

20. ABSTRACT *(Continue on reverse side if necessary and identify by block number)*

Species detectivity is limited in conventional CARS with aligned laser polarizations by the presence of a background, nonresonant electronic contribution to the CARS signal. At low species densities, a modulated CARS spectrum results which can be used to perform concentration measurements from the spectral shape, a unique feature of CARS. When the species concentration becomes very low, the 'signal' from the specie of interest, i.e. the modulation, essentially disappears into the nonresonant background and the specie is no longer detectable

DD FORM 1 JAN 73 1473 EDITION OF 1 NOV 65 IS OBSOLETE

Unclassified

SECURITY CLASSIFICATION OF THIS PAGE *(When Data Entered)*

By proper orientation of the polarizations of the pump and Stokes laser fields and the CARS signal polarization analyzer, the nonresonant background can be suppressed leaving the pure CARS spectrum of the specie being probed. Unfortunately, a factor of sixteen reduction in resonant mode signal accompanies the elimination of the background. In this report, investigations of background suppression from CO in flames are described using polarization sensitive CARS with spectrally broadband Stokes waves. The studies were conducted in flat CO-air diffusion flames employing nonplanar, crossed-beam phase matching, i.e. folded BOXCARS. The relative concentration sensitivity of CARS with and without background suppression was compared at both high and low temperatures. In all cases, the detection sensitivity of CARS with the nonresonant background present was found to be better, typically by a factor of five, than with the background suppressed. Approaches to species concentration measurements which exploit partial cancellation of the nonresonant background, and in-situ CARS reference generation from the nonresonant background are suggested. These approaches eliminate the requirement for reference cells, which may be inapplicable for CARS diagnostics in practical combustion devices due to the effects of turbulence and attenuation from soot and fuel sprays.

R80-954628-1

CARS Concentration Sensitivity with and without Nonresonant Background Suppression

TABLE OF CONTENTS

CARS Concentration Sensitivity with and without Nonresonant Background Suppression

SUMMARY

Species detectivity is limited in conventional CARS with aligned laser polarizations by the presence of a background, nonresonant electronic contribution to the CARS signal. At low species densities, a modulated CARS spectrum results which can be used to perform concentration measurements from the spectral shape, a unique feature of CARS. When the species concentration becomes very low, the "signal" from the specie of interest, i.e. the modulation, essentially disappears into the nonresonant background and the specie is no longer detectable. By proper orientation of the polarizations of the pump and Stokes laser fields and the CARS signal polarization analyzer, the nonresonant background can be suppressed leaving the pure CARS spectrum of the specie being probed. Unfortunately, a factor of sixteen reduction in resonant mode signal accompanies the elimination of the background. In this report, investigations of background suppression from CO in flames are described using polarization sensitive CARS with spectrally broadband Stokes waves. The studies were conducted in flat CO-air diffusion flames employing nonplanar, crossed-beam phase matching, i.e. folded BOXCARS. The relative concentration sensitivity of CARS with and without background suppression was compared at both high and low temperatures. In all cases, the detection sensitivity of CARS with the nonresonant background present was found to be better, typically by a factor of five, than with the background suppressed. Approaches to species concentration measurements which exploit partial cancellation of the nonresonant background, and in-situ CARS reference generation from the nonresonant background are suggested. These approaches eliminate the requirement for reference cells, which may be inapplicable for CARS diagnostics in practical combustion devices due to the effects of turbulence and attenuation from soot and fuel sprays.

INTRODUCTION

Coherent anti-Stokes Raman spectroscopy (CARS) (Refs. 1-4 and the references therein) has received considerable attention in the last several years for remote combustion diagnostics because of its potential applicability to practical systems, such as furnaces, gas turbine combustors, and internal combustion engines, over their broad operational ranges. Spontaneous Raman scattering has also been widely investigated in this regard (Refs. 5-9) and has been utilized in a number of practical situations (Refs. 9-12). However, its application is often restricted in these cases to certain fuels, stoichiometries, cycles and locations. Due to its weak signal strength and incoherent character, interferences from background luminosity (Refs. 2,9), fluorescences from fuel fragments (Refs. 9, 13-16) and/or laser-induced incandescence from soot (Refs. 17, 18) can mask detection of the Raman signals, sometimes by orders of magnitude. With visible-wavelength lasers, laser-induced or modulated soot incandescence is generally the most severe interference in hydrocarbon-fueled diffusion flames (Ref.2). Under ONR/Project SQUID sponsorship (Contract 8960-20), UTRC investigated potential solutions to interferences from laser modulated soot incandescence (Refs. 17, 19) for spontaneous Raman scattering. Based upon those investigations, it was concluded that alternative diagnostic approaches with inherently higher signal/interference ratios needed to be investigated before practical combustor probing could be realized. At that time (1977), CARS appeared the most promising of several nonlinear techniques for the diagnostic probing of high interference environments, but had not been demonstrated in particle laden situations. Under ONR/Project SQUID sponsorship (Contract 8960-28), UTRC demonstrated successful CARS temperature measurements, both averaged and single pulse, in sooting, laminar and turbulent, propane diffusion flames (Refs. 20,21). In 1979, CARS was successfully demonstrated in a number of practical combustion environments at our laboratory and others, including simulations of gas turbine combustors (Refs. 22-24) and an internal combustion engine (Ref. 25).

Another area in CARS, which needed to be addressed at the time the investigation described herein was proposed (mid 1978), concerns nonresonant susceptibility contributions to the CARS signal. These nonresonant signals, in essence, form a baseline or background level into which the CARS signal from a given species disappears at low concentration levels. For typical molecules of interest in combustion, e.g. O_2, CO, it is difficult to perform concentration measurements much below the several tenths of one percent level. The nonresonant contributions have an electronic origin as opposed to the resonant Raman terms arising primarily from the nuclear motions of the molecule. As a consequence, the nonresonant susceptibility contributions exhibit different symmetry properties and, hence, different dependences on the polarizations of the incident laser fields than do the desired resonant terms. By proper orientation of the laser field and CARS polarizations, it is possible to suppress the nonresonant electronic contributions to the CARS signals permitting, in principle, detection of species to considerably lower concentrations. Unfortunately, for symmetric Raman modes, a factor of sixteen resonant mode signal loss accompanies the cancellation of the nonresonant suscepti-

bility contributions.

At the time of our proposal, demonstrations of background cancellation were restricted to liquids (Refs. 26,27) or gases in cells (Ref. 28). Since then, demonstrations of background cancellation have occurred in flames from CO using collinear phasematching (Ref. 29) or BOXCARS (Ref. 30), and from CO_2 using BOXCARS (Ref. 22). Additional liquid-phase investigations have also been reported (Ref. 31). Background cancellation has also been reported using picosecond laser pulses with time delay between the pump and Stokes waves (Ref. 32). In all of the previous investigations, narrowband Stokes waves were used. In this report, investigations are described of polarization sensitive, nonresonant susceptibility suppression from flame CO using BOXCARS and broadband Stokes waves as would be required for measurements with both high spatial and temporal resolution. In certain concentration ranges, typically 0.1 to 20%, the presence of the nonresonant susceptibility can be exploited since it leads to spectra which are concentration sensitive, i.e. concentration measurements can be performed from spectral shapes. Because of the signal loss accompanying background cancellation together with the difficulties inherent in intensity measurements in CARS, the focus of this investigation has been upon the relative concentration sensitivity of the two approaches, i.e. with and without the nonresonant susceptibility cancelled. Attention has also been focussed on the best approach to density measurements using CARS, particularly in regard to application to practical combustors.

In the next section of this report, CARS will be briefly reviewed for completeness. Then the theory describing the polarization behavior of CARS will be presented. The CARS experimental arrangement and the burner employed will then be discussed preceeding the presentation of the experimental results. The report concludes with a discussion of the experimental results together with an examination of CARS approaches for density and concentration measurements in combustion, particularly in turbulent, particle-laden media, e.g. soot, fuel droplets.

COHERENT ANTI-STOKES RAMAN SPECTROSCOPY

Coherent anti-Stokes Raman spectroscopy (CARS) is capable of the diagnostic probing of high interference environments due to its high signal conversion efficiency and coherent signal behavior. CARS signal levels are often orders of magnitude stronger than those produced by spontaneous Raman scattering. Its coherent character means that all of the generated signal can be collected, and over such a small solid angle, that the collection of interferences is greatly minimized. CARS thus offers signal to interference ratio improvements of many orders of magnitude over spontaneous Raman scattering and appears capable of probing practical combustion environments over a broad operational range. In experiments at our laboratory and elsewhere, CARS has been successfully demonstrated in practical combustion situations. With such "real world" demonstrations, one might anticipate CARS to see widespread practical utilization in the coming years.

The theory and application of CARS are well expelained in several reviews which have appeared recently (Refs. 1-4). Briefly, as illustrated in Fig. 1, incident laser beams at fequencies ω_1 and ω_2 (often termed the pump and Stokes beams respectively) are "mixed" by focussing and crossing them appropriately and interact through the third order nonlinear susceptibility of the medium $\chi^{(3)}_{ijkl}(-\omega_3,\omega_1,\omega_1,-\omega_2)$, to generate a polarization field which produces coherent radiation at frequency $\omega_3=2\omega_1-\omega_2$. It is for this reason that CARS is often referred to as "three wave mixing". When the frequency difference $(\omega_1-\omega_2)$ is close to the frequency of a Raman active resonance, ω_v, the magnitude of the radiation at ω_3, then at the anti-Stokes frequency relative to ω_1, i.e. at $\omega_1+\omega_v$, can become very large. Large enough, for example, that with typical pulsed experimental arrangements, the CARS signals from room air N_2 or O_2 are readily visible. By third order is meant that the polarization exhibits a cubic dependence on the optical electric field strength. In isotropic media such as gases, the third order susceptibility is actually the lowest order nonlinearity exhibited,i.e. due to symmetry considerations, second order effects are nonexistent. The third order nonlinear susceptibility tensor is of fourth rank. The subscripts denote the polarization orientation of the four fields in the order listed parenthetically. In isotropic media, the tensor must be invariant to all spatial symmetry transformations and the 81 tensor elements reduce to just three independent components, χ_{xyyx}, χ_{xyxy} and χ_{xxyy} where $\chi_{xxxx} = \chi_{xyyx} + \chi_{xyxy} + \chi_{xxyy}$. In CARS, which is generally frequency degenerate, $\chi_{xyxy} = \chi_{xxyy}$ and there are only two independent elements.

As mentioned in the Introduction, the susceptibility consists of resonant components from Raman transitions in the species of interest and a nonresonant, electronic contribution from all of the molecular constituents present. For very low concentrations, the "signal", i.e. the resonant terms, merges into essentially a baseline level derived from the nonresonant background susceptibility. When the modulation of this background becomes undetectable, the trace species is nominally no longer measurable. At one time, this was perceived to be a major limitation to CARS diagnostics. However, the resonant and nonresonant terms contribute differently to the susceptibility components. By proper orientation of the laser field and CARS-detection polarizations, the nonresonant electronic contributions can be

COHERENT ANTI-STOKES RAMAN SPECTROSCOPY — CARS

- Approach

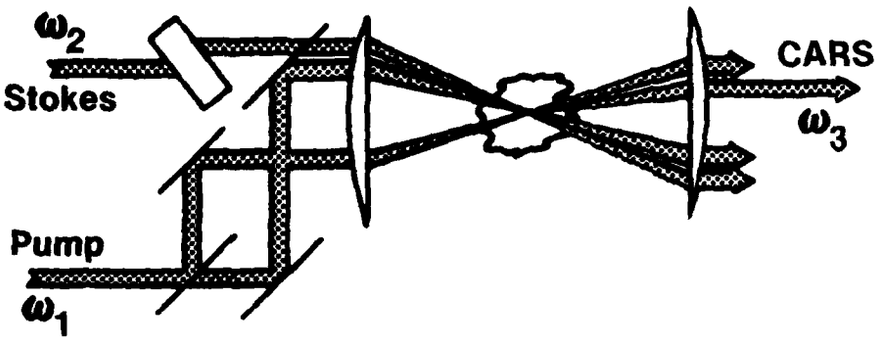

- Energy level diagram

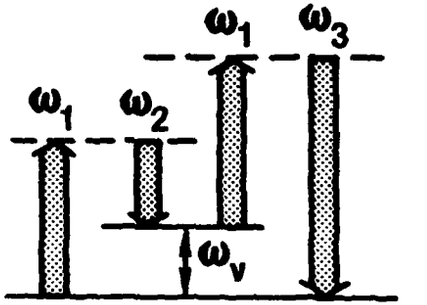

- Spectrum

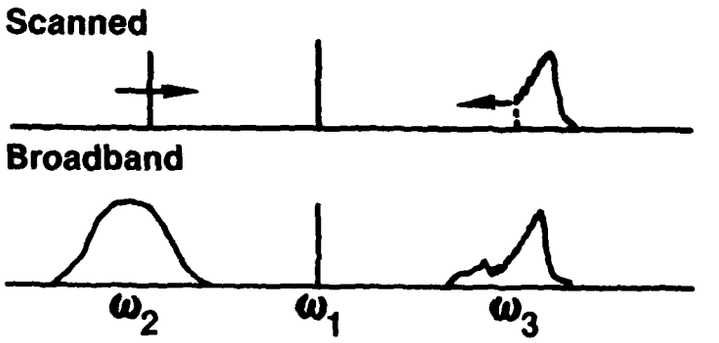

80-7-60-11

FIG. 1

suppressed, in principle, permitting measurements to lower concentration providing the signal level is adequate (Refs. 22,26-31, and this report). In certain concentration ranges, the presence of the nonresonant susceptibility can actually be used to great advantage. As long as the background modulation is detectable, concentration measurements can actually be made from the shape of the CARS spectrum, a unique feature of CARS spectroscopy. For highly turbulent and sooting media, this may be the only way in which density measurements can be accurately performed as will be discussed later. Polarization rotation may prove useful in such instances to introduce modulation or control the background level to extend the parameter range over which concentrations can be measured from spectral shapes.

Measurements of medium properties are performed from the shape of the spectral signature and/or intensity of the CARS radiation. The CARS spectrum can be generated in either one of two ways as seen in Fig. 1. The conventional approach is to employ a narrowband Stokes source which is scanned to generate the CARS spectrum piecewise. This approach provides high spectral resolution and strong signals and eliminates the need for a spectrometer. However, for nonstationary and turbulent combustion diagnostics, it is not appropriate due to the nonlinear behavior of CARS on temperature and density. Generating the spectrum piecewise in the presence of large density and temperature fluctuations leads to distorted signatures weighted toward the high density, low temperature excursions from which true medium averages cannot be obtained. The alternate approach (Ref. 33) used here is to employ a broadband Stokes source as depicted in Fig. 1. This leads to weaker signals, but generates the entire CARS spectrum with each pulse permitting, in principle, instantaneous measurements of medium properties. Repeating these measurements a statistically significant number of times will permit determination of the probability density function (pdf) from which true medium averages and the magnitude of turbulent fluctuations can be ascertained.

For efficient signal generation, the incident beams must be so aligned that the three wave mixing process is properly phased. The general phase-matching diagram for three wave mixing requires that $2\bar{k}_1=\bar{k}_2+\bar{k}_3$. $\bar{k}_i$ is the wave vector at frequency ω_i with absolute magnitude equal to $\omega_i\, n_i/c$, where c is the speed of light, and n_i, the refractive index at frequency ω_i. Since gases are virtually dispersionless, i.e., the refractive index is nearly invariant with frequency, the photon energy conservation condition $\omega_3 = 2\omega_1-\omega_2$ indicates that phase matching occurs when the input laser beams are aligned parallel or collinear to each other. In many diagnostic circumstances, collinear phase matching leads to poor and ambiguous spatial resolution because the CARS radiation undergoes an integrative growth process. This difficulty is circumvented by employing crossed-beam phase matching, such as BOXCARS (Ref. 34), illustrated in Figs. 1 and 2a, or a variation thereof (Refs. 35-37). In these approaches, the pump beam is split into two components which, together with the Stokes beam, are crossed at a point to generate the CARS signal. CARS generation occurs only where all three beams intersect and very high spatial precision is possible. Furthermore the incident beams need not be coplanar (Refs. 30, 38, 39). As seen in Fig. 2b, the phase-matching diagram can be folded, a configuration employed in the investigations reported here.

Although CARS has no threshold per se and can be generated with cw laser

FIG. 2

80-7-60-12

sources, high intensity pulsed laser sources are required for most gas phase and flame diagnostics to generate CARS signals well in excess of the various sources of interference and with good photon statistics, particularly with broadband generation and detection (Ref. 2). Due to the nonlinear scaling of the CARS signal with species concentration and temperature, CARS measurements from minority species in atmospheric pressure flames generally cannot be made with simultaneous high spatial and temporal resolution. This fact is quite evident in the experiments described herein.

CARS spectra are more complicated than spontaneous Raman spectra which are an incoherent addition of a multiplicity of transitions. CARS spectra can exhibit constructive and destructive interference effects. Constructive interferences occur from contributions made from neighboring resonances, the strength of the coupling being dependent on the energy separation of the adjacent resonances and on the Raman linewidth which together determine the degree of overlap. Destructive interferences occur when resonant transitions interfere with each other or with the nonresonant background signal contributions of electrons and remote resonances. For most molecules of combustion interest, these effects can be readily handled numerically since the physics describing CARS generation is fairly well understood. At UTRC, CARS computer codes have been developed and validated experimentally for the diatomic molecules, N_2, H_2, CO and O_2 (Ref. 40) and one triatomic H_2O (Ref. 41). Computer codes are extremely useful for studying the parametric behavior of CARS spectra and, when validated, for actual data reduction.

The species sensitivity limitation of conventional CARS, i.e. aligned polarizations, is easily demonstrated by noting that the CARS power P_3 scales as the square of the modulus of the nonlinear susceptibility $|\chi^{(3)}|^2$. The square of the absolute value of the susceptibility for a single resonance is

$$|\chi^{(3)}|^2 = |\chi' + i\chi'' + \chi^{nr}|^2$$

$$= \chi'^2 + 2\chi'\chi^{nr} + \chi^{nr2} + \chi''^2 \qquad (1)$$

where χ', χ'' are the real and imaginary parts of the resonant susceptibility and χ^{nr} is the nonresonant susceptibility. χ' and χ'' have a functional dependence on the detuning frequency, $\Delta\omega_j = \omega_j-(\omega_1-\omega_2)$, from the Raman resonance of frequency ω_j, similar to the real and imaginary parts of the refractive index about resonance. This is illustrated in Fig. 3. χ'' exhibits line shape behavior and χ' dispersive or derivative behavior, i.e. χ' is positive or negative depending on the sign of $\Delta\omega_j$. For a small nonresonant background, e.g. a species in high concentration, χ', $\chi'' > \chi^{nr}$, and $|\chi|^2$ is equal to $\chi'^2 + \chi''^2$ and the CARS spectrum exhibits strong line behavior as the detuning frequency is scanned through the resonance. For a species in low concentration, i.e. χ', $\chi'' < \chi^{nr}$

$$|\chi|^2 \approx \chi^{nr2} + 2\chi' \chi^{nr} \qquad (2)$$

and the CARS spectrum exhibits weak line behavior as seen in Fig. 3. Far from resonance, the CARS signal is proportional to χ^{nr2}. Near resonance the spectrum displays a modulated behavior due to the change in sign of χ' about resonance. For very low concentrations, the "signal" disappears into essentially a baseline level

CARS SPECTRAL BEHAVIOR

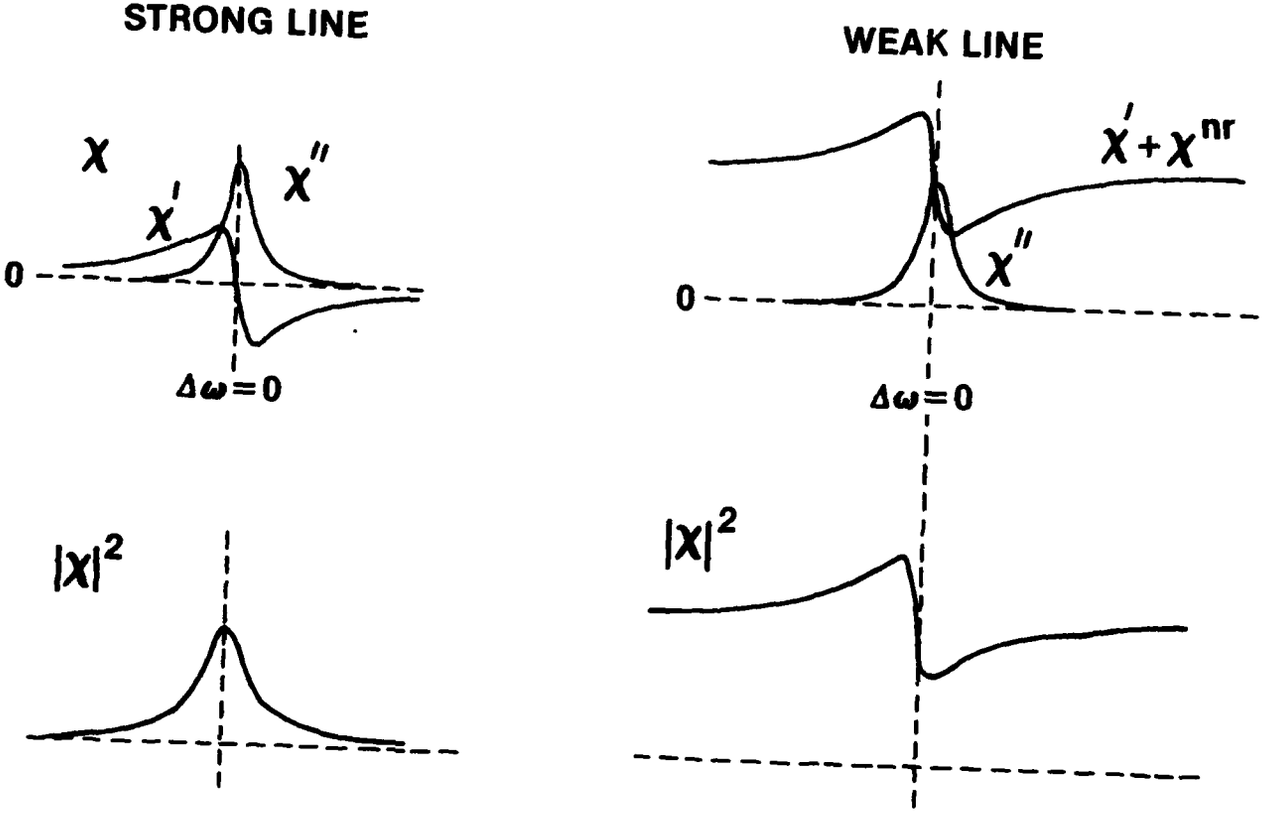

FIG. 3

80-7-60-13

derived from the background nonresonant susceptibility. When the modulation of this background becomes undetectable, the trace species concentration is no longer measurable. Detailed computer calculations of CO at various concentrations in a flame display this sensitivity limitation effect vividly as seen in Fig. 4. A complete set of computer calculations over a matrix of temperature and CO concentration is displayed in Appendix A. The rounded nature of the spectrum reflects the profile assumed for the Stokes laser at ω_2. Experimentally, it would be difficult to detect CO at concentrations below the 0.5% level in a flame. Nevertheless, where modulation exists the concentration can be measured from the spectral signature which is far easier than performing an intensity measurement with normalizing reference cells. Furthermore in turbulent media, the latter approach may not be very accurate as will be discussed later in this report.

The concentration measured from the shape of the modulated spectrum is only as accurate as the accuracy to which the nonresonant background susceptibility is known (Ref. 40). The nonresonant susceptibility has been measured for most of the gases of combustion interest and varies slightly from specie to specie (Ref. 42 and Table A-I in Appendix A). In airfed combustion wheren N_2 dominates the composition, the change in the nonresonant susceptibility from the reactant to product mixture is generally small. In CH_4/air combustion, for example, the susceptibility increases by about 14% with combustion of the stoichiometric mixture. The susceptibility is thus only slightly sensitive to changes in composition and intelligent estimates of its magnitude are most likely possible based upon the temperature at the measurement point.

To overcome the loss in species sensitivity when the modulation of the nonresonant background is no longer discernible, several approaches have been forwarded (Refs. 26-32, 43-45). The best approach at this time, in terms of simplicity, is probably polarization orientation which is described in the next section and forms the basis of the experimental program reported herein.

CONCENTRATION SENSITIVITY OF CO CARS SPECTRA

T = 1800 °K, Ar background

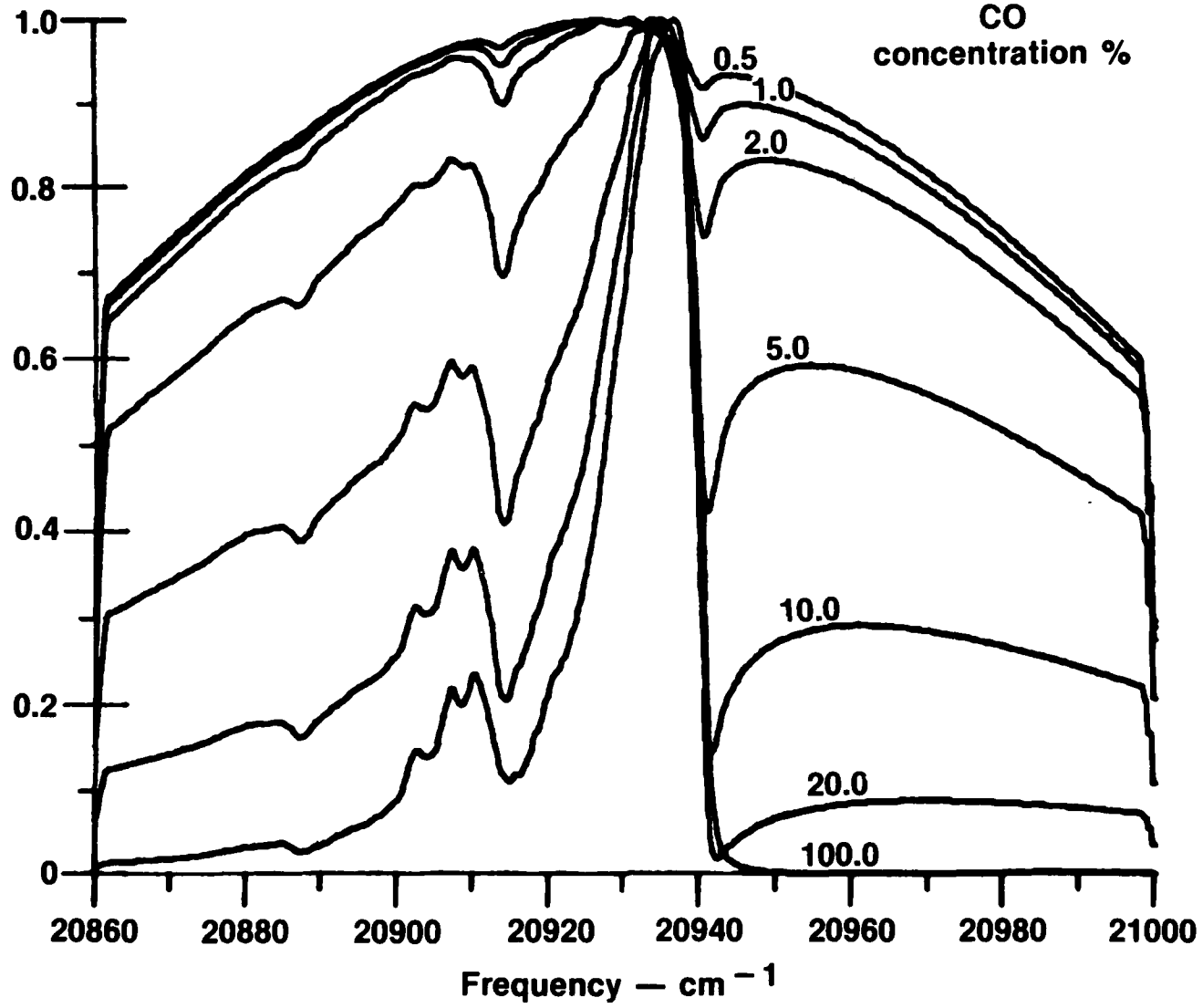

FIG. 4

80-7-60-18

POLARIZATION ORIENTATION

The third order nonlinear susceptibility tensor $\chi^{(3)}_{ijkl}(-\omega_3, \omega_1, \omega_1', -\omega_2)$ is fourth rank in order. The subscripts denote the polarization directions of the four fields in the order listed in the parentheses. In isotropic media, the tensor must be invariant to all spatial symmetry transformations and the 81 tensor elements reduce to three independent elements, χ_{1221}, χ_{1212}, and χ_{1122} where $\chi_{1111} = \chi_{1221} + \chi_{1212} + \chi_{1122}$. The superscript (3) has been dropped for simplicity. For normal CARS, which is frequency degenerate i.e. $\omega_1 = \omega_1'$, there are only two independent elements since $\chi_{1212} = \chi_{1122}$ (Ref. 46). From Ref. 46 it is possible to show (Ref. 29) that

$$\chi_{1111} = \frac{1}{24} (3\sigma + 4a + 4b)$$

$$\chi_{1221} = \frac{1}{24} (\sigma + 2b) \qquad (3)$$

$$\chi_{1212} = \chi_{1122} = \frac{1}{24} (\sigma + 2a + b)$$

where σ represents the fast responding electronic contribution (i.e. the nonresonant contribution to the susceptibility) and a and b are the nuclear response functions. For Raman type nonlinearities, a and b relate respectively to the isotropic and anisotropic parts of the Raman polarizability derivative tensor.

By considering the field orientation in Fig. 5 for BOXCARS, it will be shown that by suitably selecting the angles θ, φ and α, the nonresonant electronic terms need not be viewed. In the calculations, it is assumed that the Stokes field is horizontally polarized along the x axis and that the pump components ω_1' and ω_1 are inclined to the Stokes field at angles φ and θ respectively. The CARS signal is viewed through a polarization analyzer oriented at angle α to the Stokes field. The fields may be written as

$$\vec{E}_i = A(\omega_i) e^{i(k_i z - \omega_i t)} + \text{complex conjugate} \qquad (4)$$

where $A(\omega_i)$ is the field amplitude at frequency ω_i. The field components of the incident waves along the y and x axis are:

	ω_1	ω_1'	ω_2
y	$A(\omega_1) \sin\theta$	$A(\omega_1') \sin\varphi$	0
x	$A(\omega_1) \cos\theta$	$A(\omega_1') \cos\varphi$	$A^*(\omega_2)$.

(5)

CARS POLARIZATION ORIENTATION DIAGRAM

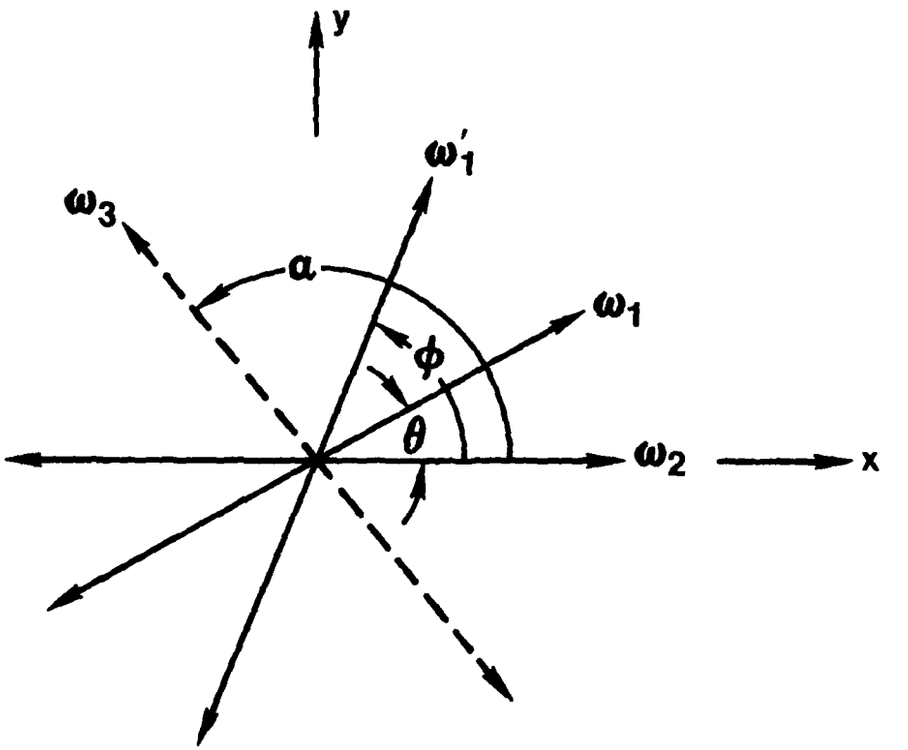

FIG. 5

80-7-60-9

The third order CARS polarization is given by

$$P_i = 3\,\chi_{ijkl}\,A_j(\omega_1)\,A_k(\omega_1')\,A_l^*(\omega_2) \qquad (6)$$

hence

$$P_x = 3A(\omega_1)\,A(\omega_1')\,A^*(\omega_2)\left[\chi_{xxxx}\cos\theta\cos\varphi + \chi_{xyyx}\sin\theta\sin\varphi\right] \qquad (7)$$

$$P_y = 3A(\omega_1)\,A(\omega_1')\,A^*(\omega_2)\left[\chi_{yxyx}\cos\theta\cos\varphi + \chi_{yyxx}\sin\theta\cos\varphi\right].$$

The CARS signal field strength is given by

$$\vec{A}(\omega_3) = \frac{2\pi i\omega_3 l}{n_3 c}\left\{\vec{P}_x + \vec{P}_y\right\} \qquad (8)$$

where l is the interaction length; n_3, the refractive index at frequency ω_3; and c, the speed of light. Viewed through the polarizer at angle α the detected CARS field is

$$\left[\vec{A}(\omega_3)\right]_\alpha = \frac{2\pi i\omega_3 l}{n_3 c}\left\{P_x\cos\alpha + P_y\sin\alpha\right\} \quad . \qquad (9)$$

Combining Eqs. (3), (7) and (9) one has

$$\frac{\left[\vec{A}(\omega_3)\right]_\alpha}{\left(\frac{2\pi i\omega_3 l}{n_3 c}\right)A(\omega_1)A(\omega_1')A^*(\omega_2)} = \qquad (10)$$

$$\frac{a}{8}\left\{4\cos\alpha\cos\theta\cos\varphi + 2\sin\alpha\cos\theta\sin\varphi + 2\sin\alpha\sin\theta\cos\varphi\right\}$$

$$+\frac{b}{8}\left\{4\cos\alpha\cos\theta\cos\varphi + 2\cos\alpha\sin\theta\sin\varphi + \sin\alpha\cos\theta\sin\varphi + \sin\alpha\sin\theta\cos\varphi\right\}$$

$$+\frac{\sigma}{8}\left\{3\cos\alpha\cos\theta\cos\varphi + \cos\alpha\sin\theta\sin\varphi + \sin\alpha\cos\theta\sin\varphi + \sin\alpha\sin\theta\cos\varphi\right\}$$

Since CARS is frequency degenerate, one will note that the above equation is unaltered by an interchange of the angles θ and φ. Clearly, the nonresonant contribution will not be detected when the coefficient of σ in brackets is nulled, i.e.

$$\cos\alpha\,(3\cos\theta\cos\varphi + \sin\theta\sin\varphi) + \sin\alpha\,(\cos\theta\sin\varphi + \sin\theta\cos\varphi) = 0 \quad . \qquad (11)$$

It should be stressed that α, θ and φ are not all independent variables. The proper polarization analyzer orientation, α, is dependent upon the experimenter's selection of θ and φ. Physically the CARS analyzer is positioned to be orthoganal to the nonresonant polarization created in the medium. It is important to note that, in general, a nonresonant contribution is generated. By properly orienting the CARS polarizer, it is simply not viewed. Combining Eqs. (3) and (7) and retaining only the nonresonant contributions, the nonresonant polarization components are

$$\frac{P_x^{nr}}{3A(\omega_1)A(\omega_1')A^*(\omega_2)} = \frac{\sigma}{8}\left[\cos\theta\cos\varphi + \frac{\sin\theta\sin\varphi}{3}\right]$$

$$\frac{P_y^{nr}}{3A(\omega_1)A(\omega_1')A^*(\omega_2)} = \frac{\sigma}{24}\left[\cos\theta\sin\varphi + \sin\theta\cos\varphi\right] \qquad (12)$$

The nonresonant polarization resides inclined at an angle β relative to the x or Stokes field axis given by

$$\beta \equiv \measuredangle P^{nr} = \tan^{-1}\frac{P_y^{nr}}{P_x^{nr}} = \tan^{-1}\left\{\frac{\cos\theta\sin\varphi + \sin\theta\cos\varphi}{3\cos\theta\cos\varphi + \sin\theta\sin\varphi}\right\} \qquad (13)$$

The polarization analyzer angle α is set orthogonally to the nonresonant polarization so the purely electronic contributions are not viewed

$$\alpha = \beta + 90^\circ \quad . \qquad (14)$$

Having selected θ and φ, the analyzer orientation for zero nonresonant susceptibility contribution is thus determined. θ and φ are selected to maximize the viewed CARS signal strength, i.e. the a coefficient in Eq. (10). Inserting Eq. (11) into the expression for the coefficient of a, and ignoring the anisotropic contribution, one obtains

$$\frac{\left|\vec{A}(\omega_3)\right|_\alpha}{\left(\frac{2\pi i\omega_3 l}{n_3 c}\right)A(\omega_1)A(\omega_1')A^*(\omega_2)} = -\frac{1}{4}\cos\alpha\cos(\theta - \varphi) \quad . \qquad (15)$$

The CARS intensity scales as the square of the field strength and, hence, is proportional to the square of the right hand side of Eq. (15). With the nonresonant susceptibility cancelled out, the a^2 coefficient has a maximum value of 0.015625. With aligned polarizations, ignoring nonresonant contributions, the a^2 modulus is 0.25. Thus with the proper polarization orientations, elimination of the nonresonant

susceptibility contribution leads to at least a factor of sixteen reduction in the resonant mode CARS signal. The analysis also shows that there is no signal advantage in polarization orientation BOXCARS with three beams over the two beam collinear CARS case (Ref. 29).

There is one respect,however, in which polarization orientation in BOXCARS differs from the usual two beam collinear situation. In the latter instance, a nonresonant signal is always generated. In BOXCARS, there is a specific angular orientation in which no signal is generated from the nonresonant background at all, i.e. it is completely cancelled. Note that no nonresonant susceptibility signal will be generated if the terms in parentheses in Eq. (11) are both made to equal zero, i.e.

$$\begin{aligned} 3\cos\theta\cos\varphi + \sin\theta\sin\varphi &= 0 \\ \cos\theta\sin\varphi + \sin\theta\cos\varphi &= 0 \end{aligned} \qquad (16)$$

This occurs when $\varphi = 60^{\circ}$, $\theta = 120^{\circ}$ or vice versa. In this instance no signal is generated from the background susceptibility and a CARS polarization analyzer is not necessary. To reiterate, there is no gain in the resonant CARS signal strength, however.

There are a large number of θ, φ angle combinations one can use to eliminate the nonresonant susceptibility contribution and obtain maximum CARS signal strength. In Table I, calculations of θ, φ, α and a^2 modulus are presented for nonresonant susceptibility cancellation. These calculations are summarized in Figs. 6 and 7 in a topographical format. In Fig. 6, due to the interchangability of θ and φ, the contours are symmetric about a 45° axis as seen. As is apparent there is a large area in angle space in which the nonresonant susceptibility can be eliminated while maintaining the maximum CARS generation. The locus $\theta = \varphi$ represents the CARS signal variation with polarization cancellation in normal two beam or collinear CARS.

TABLE I

ORIENTATION ANGLES FOR MAXIMUM CARS GENERATION
WITH NONRESONANT SUSCEPTIBILITY CANCELLATION
$\measuredangle(\omega_2) = 0^\circ$

$\theta(\omega_1)$	$\phi(\omega_1')$	$\alpha(\omega_3)$	a^2	$\hat{a}^2$
60	0	120	.00391	.25
120	0	60	.00391	.25
60	5	120	.00514	.33
65	10	124.5	.00659	.36
70	15	128.9	.00811	.52
70	20	127.9	.00973	.62
75	25	131.5	.01135	.73
80	30	134.9	.01286	.82
80	35	132.4	.01422	.91
85	40	134.3	.01522	.97
90	45	135	.01563	1
75	50	123.5	.01561	1
65	55	120.5	.01562	1
115	55	175	.01551	.99
60	60	120	.01563	1
120	60	no analyzer req'd	.01563	1
55	65	120.5	.01562	1
125	65	5	.01551	.99
50	70	122.1	.01560	1
130	70	10	.01515	.97
50	75	123.5	.01561	1
130	75	29.7	.01552	.99
45	80	127.6	.01559	1
135	80	29.8	.01550	.99
45	85	130.7	.01562	1
135	85	38.9	.01562	1
45	90	135	.01563	1
135	90	45	.01563	1

POLARIZATION ANGLES FOR BACKGROUND-FREE CARS

CARS analyzer angles not shown; relative CARS amplitude as % of maximum background-free signal

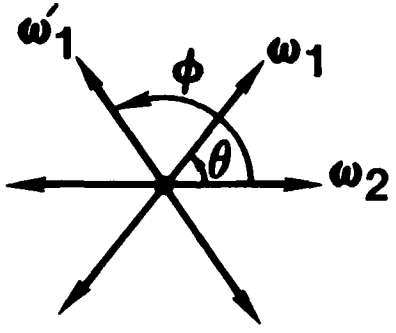

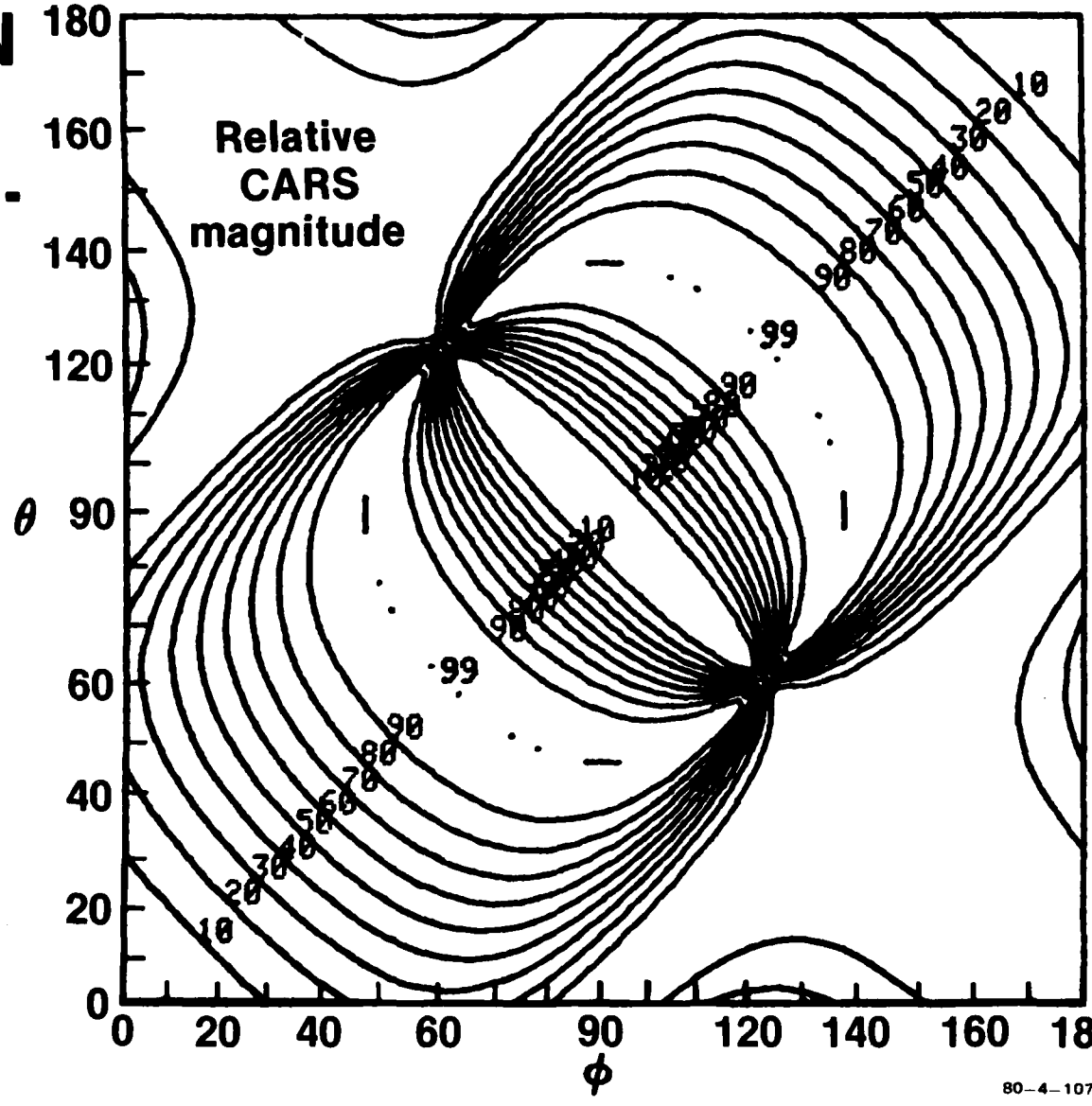

80-4-107-1

FIG. 6

CONTOUR PLOT OF BACKGROUND-FREE, RESONANT CARS SIGNAL AMPLITUDE

$\measuredangle\, \omega_2 = 0°, \omega_1(\theta), \omega'_1(\phi)$, CARS analyzer $\measuredangle$ not displayed

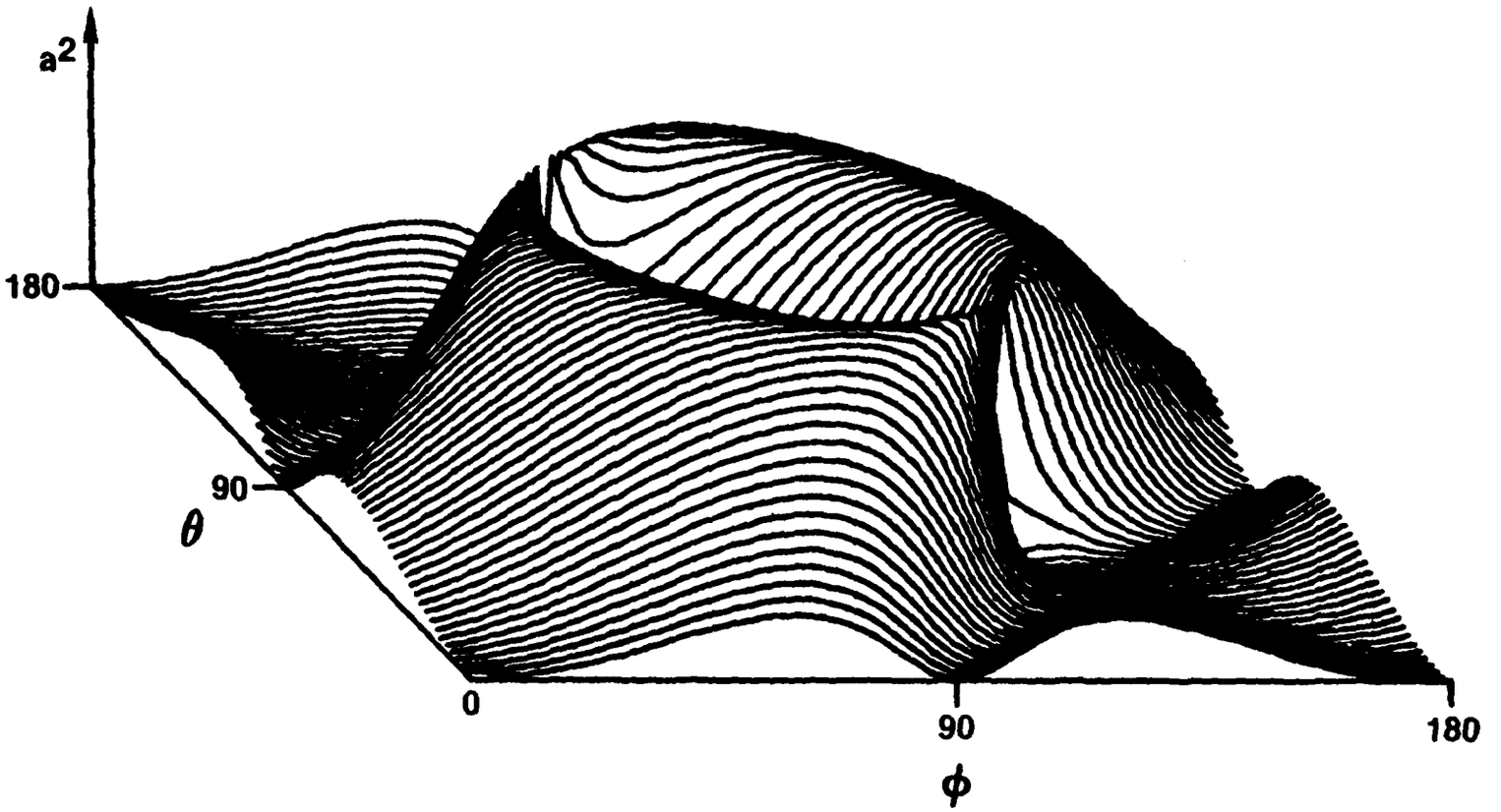

FIG. 7

80-7-60-10

EXPERIMENTAL FACILITY

The CARS facility employed for the polarization orientation investigations is schematically illustrated in Fig. 8. A photograph of the experimental apparatus is shown in Fig. 9. Referring to Fig. 8, a Q-switched neodymium:YAG laser (Quanta-Ray DCR 1A) is frequency-doubled to produce a primary beam at 5320 Å, ω_{1p}, with the following characteristics: $\sim$ 200 mJ pulse energy, 10^{-8} sec pulse duration and 10 pps repetition rate. The residual 1.06μ from the first frequency doubler is separated from the primary 5320 Å and doubled to produce a secondary beam, ω_{1s}, of approximately 20 mJ energy. This beam is routed as shown and used to pump, slightly off-axis, a flowing dye cell situated in a planar Fabry-Perot oscillator cavity. The oscillator output is amplified in a dye cell in flow series with the first,pumped by a fraction, $\sim$33%, of the primary ω_{1p} beam. The Stokes output so produced is typically 160 cm^{-1} FWHH. Since no dispersion is present in the broadband dye oscillator cavity, the Stokes frequency is appropriately centered by proper selection of the laser dye and its concentration. To obtain good laser efficiency at $\sim$ 6500 Å required for CO CARS, a binary dye mixture of 1 (10^{-4}) M Kiton Red 620 3 (10^{-5}) M Rhodamine 640 (Ref. 47) in methanol was employed. Although the dye cells are oriented at Brewster's angle and nominally produce a horizontally polarized beam, a Glan laser polarizer is employed to ensure a high degree of polarization purity. The Stokes beam is magnified in a Galilean telescope by a factor of three to ensure that its focal spot size is comparable to that of the ω_1 pump components. The telescopes also allow the beam waist location to be placed at the crossing point. The remaining ω_{1p} primary beam is also filtered by a Glan laser polarizer, passes through a telescope, where it is reduced slightly, and then to a beamsplitter/mirror combination to produce the two pump components required for BOXCARS. As mentioned earlier, folded, i.e. nonplanar, BOXCARS is employed to eliminate the need for beam combining and separating dichroics or prisms which can produce elliptically polarized beams or which possess considerably different response to s and p polarization components. The two pump components, ω_1' and ω_1, pass through low-order half wave plates which permit the plane of polarization to be oriented as desired, i.e. θ and ϕ adjustment. The pump components are reflected from semicircular mirror segments whose straight edges are oriented at 45° to the horizontal plane. Viewed head on from the focussing lens, FL, the mirrors form a "VEE" through which the Stokes laser beam passes. The beams were aligned on a 1.3 cm diameter circle and focussed with a 30.5 cm focal length lens corresponding to a crossing half angle of approximately 1.2°. A rotatable optical flat,ROF was placed in the Stokes beam. Rotation about a horizontal axis laterally displaced the Stokes beam on the focussing lens permitting the optimal phase matching angle to be ascertained. The longitudinal spatial resolution, measured by generating CARS in a translatable microscope slide cover, was approximately 0.9 cm. The laser and newly-generated CARS beams were recollimated by a lens, RL. The laser beams were blocked by a trap and the CARS beam passed through a Glan-Thompson polarizer placed directly after the trap. The CARS beam passed through a cutoff filter to reject any stray laser light and was focussed into a homemade, 0.5m Czerny-Turner spectrograph fitted with an optical multichannel analyzer (OMA I, PAR Inc). The spectrograph was equipped with a flat 2400 groove/mm holographic grating. The spectrograph was in essence an over-and-under Czerny Turner configuration turned 90°, i.e. the slit was horizontally disposed and the grating

FIG. 8

SCHEMATIC OF CARS EXPERIMENTAL ARRANGEMENT

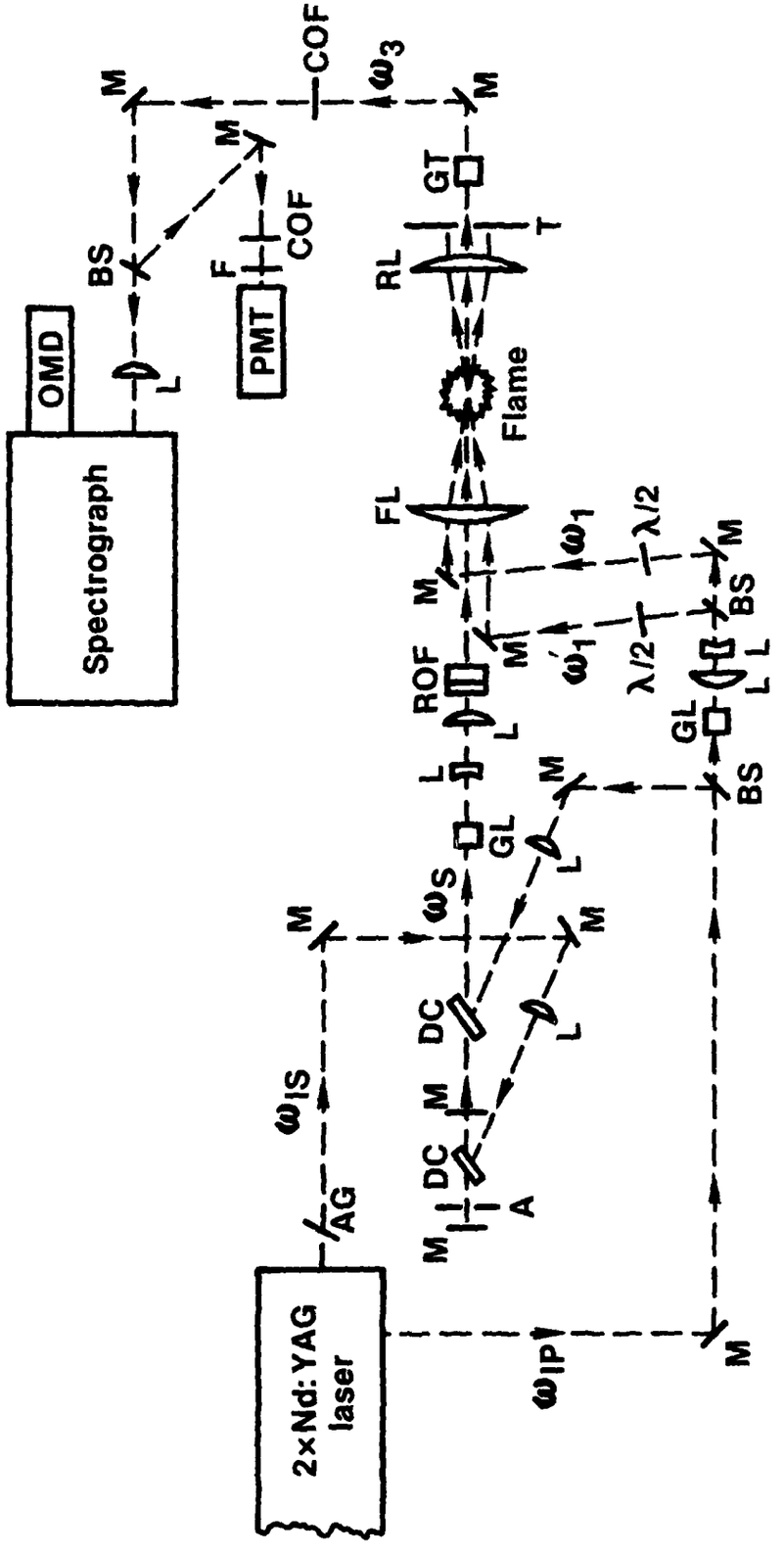

80-7-60-1

FIG. 9

FOLDED BOXCARS FACILITY

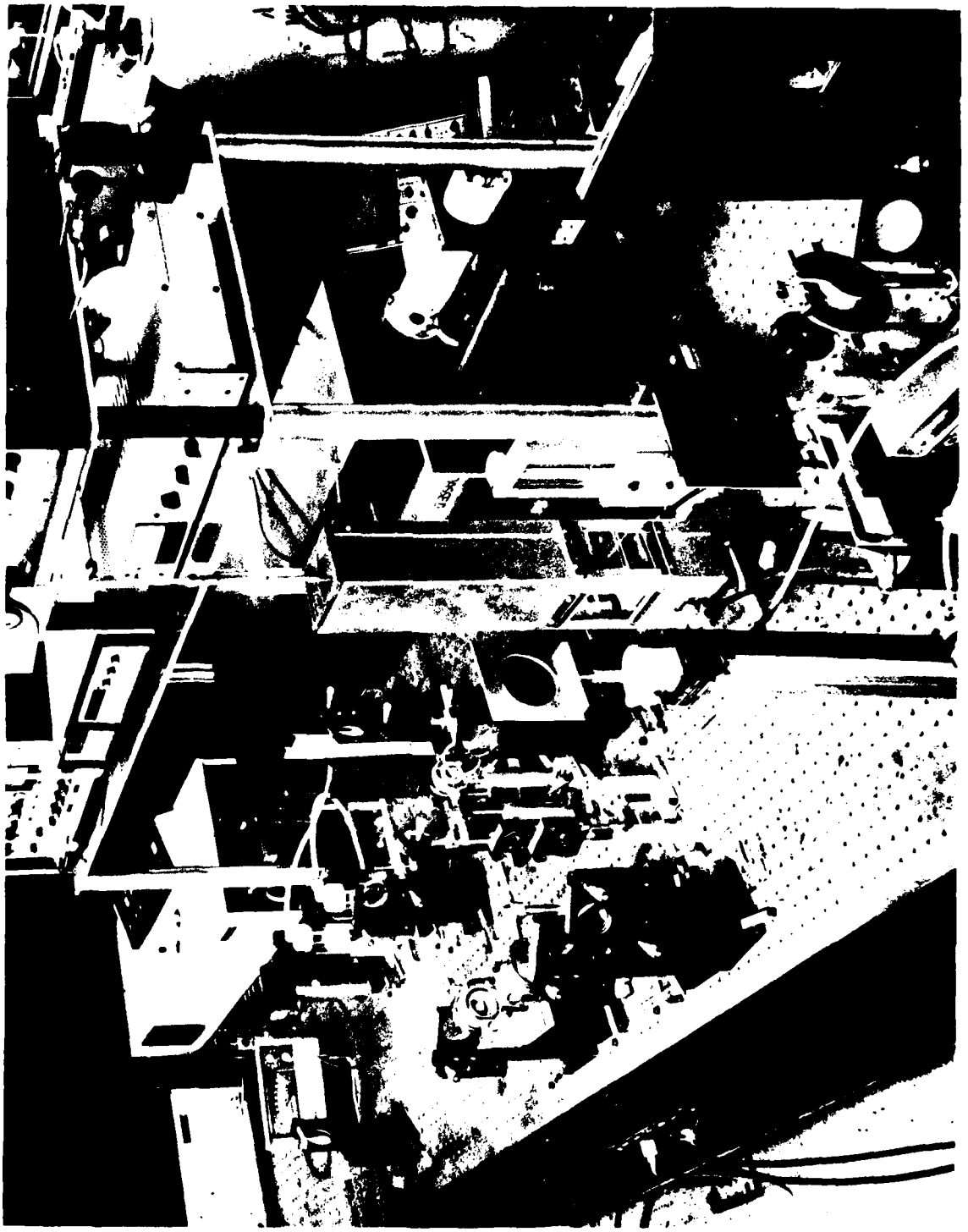

80-206-A

80-7-60-3

axis was horizontal. The dispersion was approximately 0.48 $cm^{-1}/25\mu$ channel element. With a 50μ slit, the resultant spectral resolution, degraded by cross-talk on the multichannel detector vidicon, was slightly better than 2 cm^{-1}. A microscope slide beamsplitter intercepted a fraction of the CARS signal which was monitored by a photomultiplier tube equipped with a cuttoff and narrowband interference filter. This detector has a large angular acceptance and its output, averaged on a boxcar averager (PAR 162/164), permitted the optical alignment of the CARS system to be adjusted for maximum signal generation.

To produce varying concentrations of CO at varying temperatures to investigate the detectivity limits with and without the nonresonant background, a flat CO-air diffusion flame sustained on a Wolfhard-Parker burner (Ref. 48) was employed. CO and air issue from parallel rectangular slots, diffuse together and react. The slots had a length of 44.5 mm and widths of 1.2 mm for CO and 2.7 mm for the air; the stainless steel splitter plate separating the two slots was 0.9 mm thick. The flowrates employed were 12 liters/min for air and 2.8 liters/min for CO. The resultant cold flow velocities were approximately 167 cm/sec for the air and 88 cm/sec for the CO. At these flow velocities, the vee-shaped flame sheet, as perceived by the blue luminosity, was centered about a vertical plane over the splitter plate. To promote flame stability, a shield gas flow is employed and confined inside a chimney as seen in Fig. 9. Either Ar or N_2 were employed as the shield gases. In Fig. 10 a photograph of the flame viewed normal to the reaction zone plane is displayed. The CARS measurement location was located at a fixed point in space and the burner was translated permitting various parts of the flame zone to be probed. CO decay can be followed at low temperatures as the CO diffuses into the cold shield gas on one side or at high temperature as the CO diffuses into the air and reacts. Also seen in Fig. 10 was a quartz microprobe used to sample CO at various locations in the flame. A Beckman Model 864 CO Infrared Analyzer was employed to measure the CO content in the sampling stream. As will be seen later, the probe perturbed the delicate, flat diffusion flame and could not be used. Consequently, the CARS measurements were calibrated relative to the probe in the post-flame region of a 7.5 cm dia. premixed, flat flame burner constructed from an array of 0.3 cm dia. stainless steel hypo tubes.

FIG. 10

CO-AIR FLAT DIFFUSION FLAME

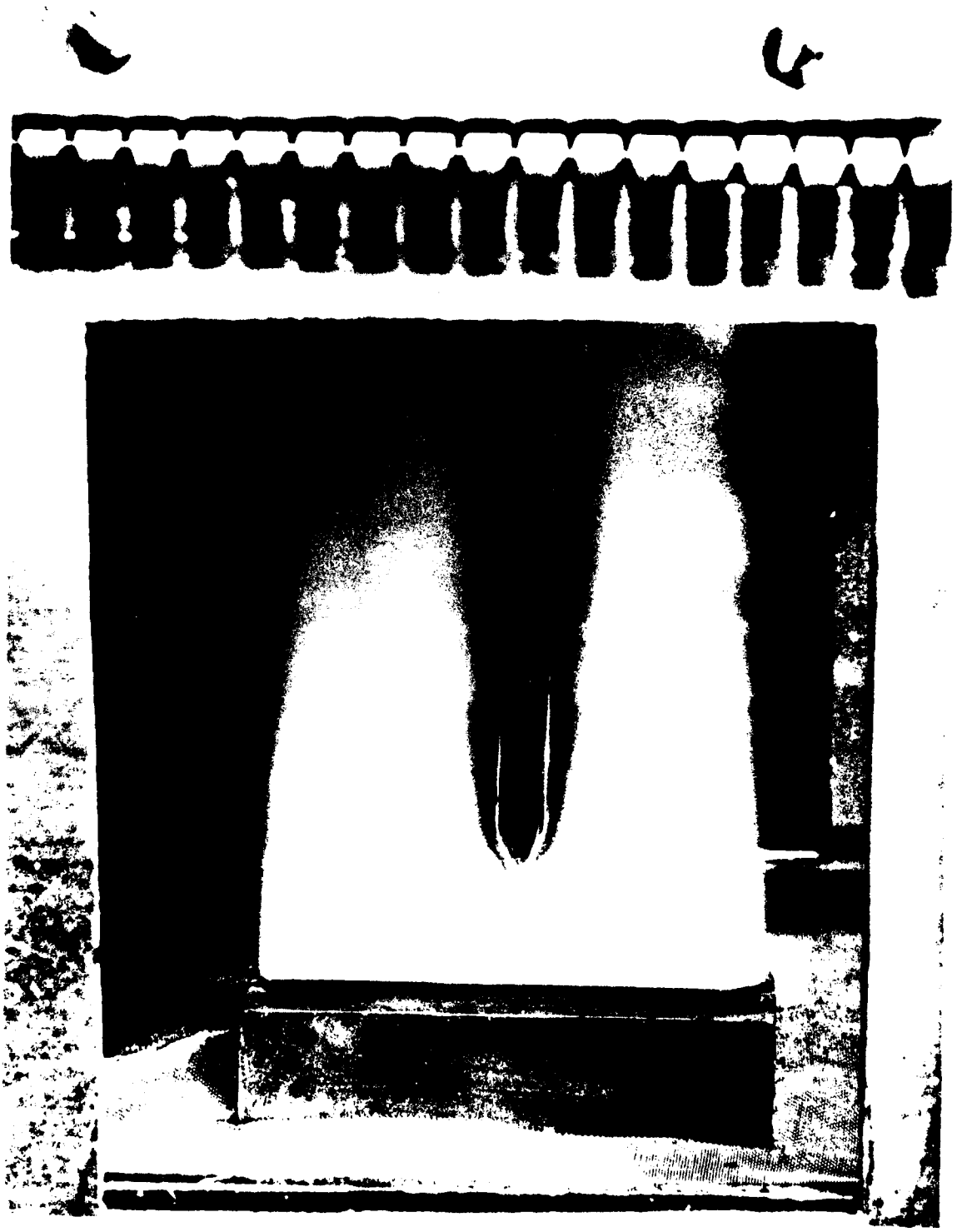

80-206-8

80-7-60-4

EXPERIMENTAL PROGRAM

Nonresonant Susceptibility Suppression

Demonstrations of nonresonant susceptibility suppression were performed in the cool region of the flat diffusion flame where CO was diffusing into the diluent shield gas. Background-free CARS spectra at elevated temperatures will be displayed subsequently in the section describing detectivity comparisons. The half-wave plates in each of the pump component beams (Fig. 8) were mounted in rotation stages, whose settings for a given polarization orientation were tabulated. The Glan Thompson CARS polarization analyzer was also mounted in a rotation stage and the appropriate angles measured and recorded. Examples of nonresonant susceptibility suppression in broadband CARS are displayed in Figs.11-13. The spectra shown have been averaged for 30 seconds or approximately 300 pulses. The ordinate axis displays the average number of optical multichannel detector counts per pulse. There are approximately 12 photons per count. In each case, the CARS spectrum with aligned polarizations is shown for comparison purposes and has the classical modulated character described earlier in the report and shown in Appendix A. In Fig. 11, background suppression is displayed with Argon as the diluent for a commonly used angle combination of $\theta = \phi = 60^{o}$, $\alpha = 120^{o}$ (Refs. 22, 29). The CO concentration was approximately 1.2% as determined from the modulated spectral shape. With the nonresonant susceptibility suppressed, the CARS spectrum is simply the cold, Q-branch band of CO. From the FWHH of the spectrum, the temperature can be determined and is just below 400°K. The width of the baseline with background cancellation arises from the quantum statistics of the dark current subtraction procedure with the OMA I. In 30 seconds, there are approximately 25 (10^3) dark current counts which would have a statistical variation of $[25\ (10^3)]^{\frac{1}{2}}$ or $\pm$ 158. Subtracting dark current sampled with the Stokes beam blocked to preclude CARS generation, from the CARS signal plus dark current, leads to a statistical spread in the baseline of $\pm$ 316 counts over 30 seconds (300 laser pulses) or approximately $\pm$ 1 count/pulse. With the uncertainty in the baseline, the background reduction is, conservatively, at least a factor of 250. Also quite apparent is the reduction in CARS signal strength attendent with elimination of the nonresonant susceptibility. The actual reduction encountered is a function of the specific experimental setup employed here and incorporates the polarization sensitivity of the individual components in the optical train. Here most of the sensitivity resided in the holographic grating in the spectrograph which was nearly four times more efficient with s (vertical) polarization than with p (horizontal). Hence the actual signal reduction is greater than the factor of 20 seen and is more like 80. This follows since the resonant mode signal loss with nonresonant susceptibility suppression is a factor of sixteen. In addition, there is the signal loss associated with the nonresonant susceptibility contribution itself.

In Fig. 12, nonresonant susceptibility suppression is shown with N_2 as the diluent shield gas and with the angles $\theta = 45^{o}$, $\phi = 90^{o}$ and $\alpha = 135^{o}$. The situation is very similar to that of Fig. 11, but two items are worth noting. Because of the proximity of the CO vibrational Raman mode at 2143 cm^{-1} to that of N_2 at 2331 cm^{-1}, the off-resonant susceptibility from N_2 contributes significantly to the nonresonant

FIG. 11

NONRESONANT SUSCEPTIBILITY SUPPRESSION IN FLAT DIFFUSION FLAME WITH ARGON DILUENT

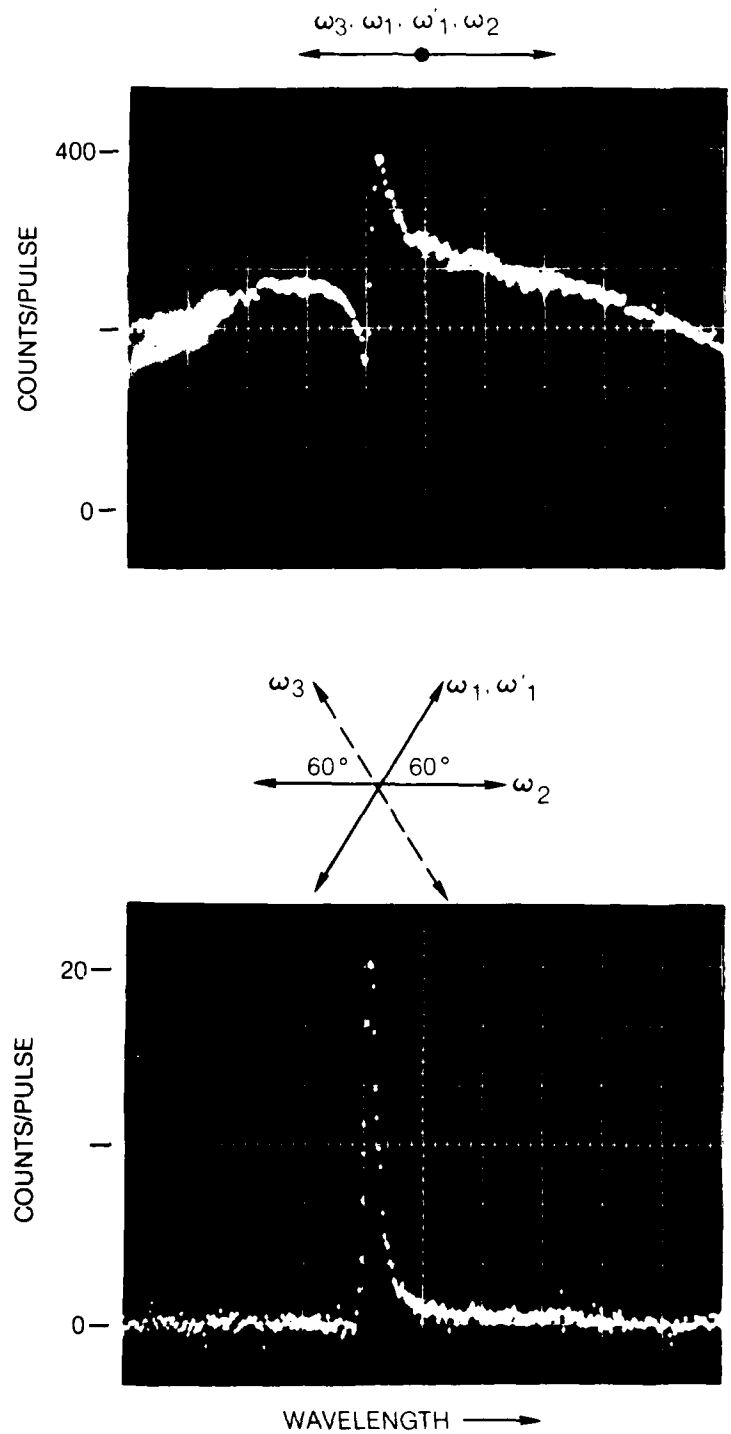

80-4-107-3

FIG. 12

NONRESONANT SUSCEPTIBILITY SUPPRESSION IN FLAT DIFFUSION FLAME WITH NITROGEN DILUENT

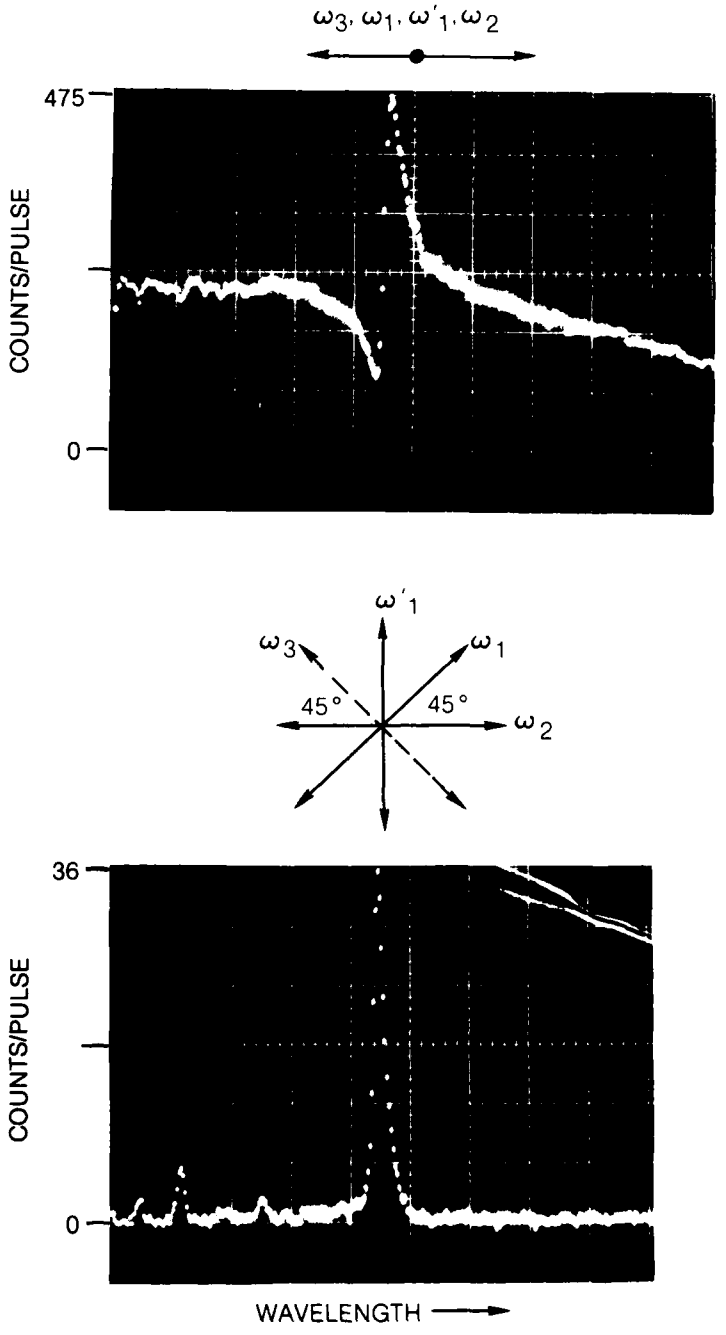

80-4-107-2

NONRESONANT SUSCEPTIBILITY CANCELLATION WITH NO CARS ANALYZER

Folded BOXCARS in a flat CO-air-Ar diffusion flame

$T \approx 400°K$ $CO \sim 1.2\%$

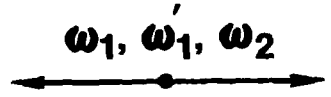

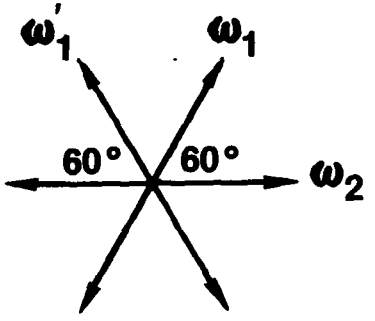

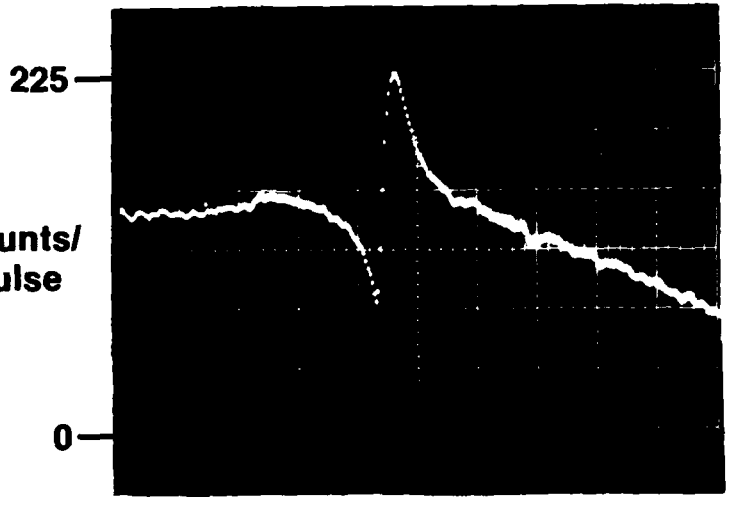

Pulses averaged: 160

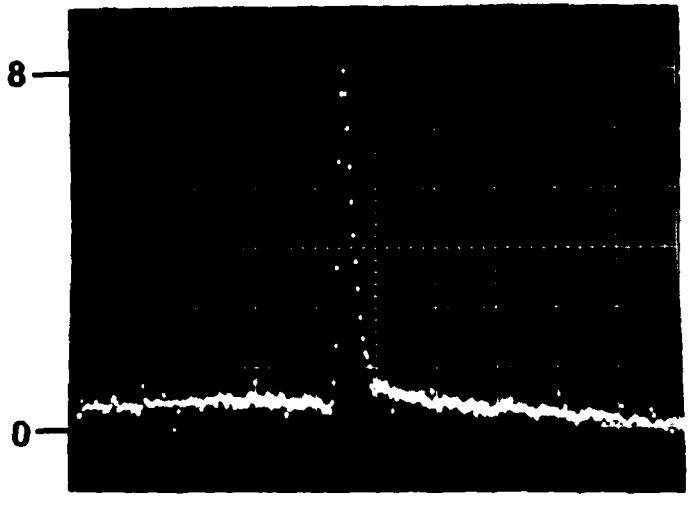

300

FIG. 13

80-7-60-2

susceptibility, i.e. by about 20%, and skews the modulated spectrum as seen. The off-resonant susceptibility of N_2 is the value of the resonant susceptibility far off resonance. Also apparent, adjacent to the Q-branch bandhead of CO, are several O branch transitions in N_2 in the vicinity of the CO resonance. A similar observation was made in Ref. 29.

In Fig. 13 nonresonant susceptibility cancellation (or near cancellation) is demonstrated for $\theta = 60^o$ and $\phi = 120^o$. In this orientation, no signal, in principle, is generated from the nonresonant susceptibility at all and a CARS polarization analyzer is not required. Recall that this is a situation unique to three beam CARS schemes. The Fig. 13 data were taken with the polarization analyzer removed. As can be seen, the degree of nonresonant susceptibility reduction is not as good as in the previous two instances. Since there is no signal advantage to be gained from this approach, all further studies were conducted with a polarization analyzer and the angles $\theta = \phi = 60^o$.

Flat Flame Probe Perturbation

In an effort to ascertain the detectivity limits of CARS with and without the background present, quartz microprobe surveys of CO concentration through the flat diffusion flame were made. The microprobe was not cooled and was 0.63 cm in O.D.. The probe was tapered at the end and contained a 400μ dia. orifice. CARS surveys of CO concentration with and without the nonresonant susceptibility present were also performed. In comparing the various sets of data, the probe surveys were clearly questionable. For example, if taken literally, the probe results suggested comparable detectivity limits for CARS at flame temperatures as around room temperature. For a constant pressure flame, this clearly cannot be the situation since the density changes accompanying combustion result in greatly reduced CARS signal levels. This fact is illustrated in Fig. 14 where the results of CARS computer code calculations are summarized. Plotted on the ordinate is the square of the modulus of the susceptibility appropriately convoluted (Ref. 40) over the finite bandwidths of the pump (0.8 cm^{-1}) and Stokes lasers (150 cm^{-1}). CARS signal powers can be found by multiplying the ordinate value at the approproate temperature by the factor in brackets. The signal levels at other concentrations can be approximated by scaling the signal with the square of the fractional concentration. The signal level calculation should also reflect system collection efficiencies and the fact that experimental signal levels are typically lower than calculated by as much as an order of magnitude (Refs. 3,4, 24). Plotted is both the peak intensity and integrated bandstrength of nonresonant-background-free CO CARS spectra as a function of temperature. For recording by an optical multichannel detector where the spectrum is dispersed, the scaling of the peak intensity with temperature is most relevant. As seen the peak intensity decreases by a factor of 400 in going from 300^oK to 1800^oK at constant pressure. Background-free CARS sensitivities are limited by photon level considerations; thus, flame and cold gas detectivities should differ considerably. Since the CARS power scales roughly as the second power of the concentration, cold side detectivities should be approximately twenty times better than those at flame temperatures. In lieu of the anomolous behavior suggested by the sampling probe, the probe measurements were certainly suspicious.

FIG. 14

CO CARS POWER VARIATION WITH TEMPERATURE

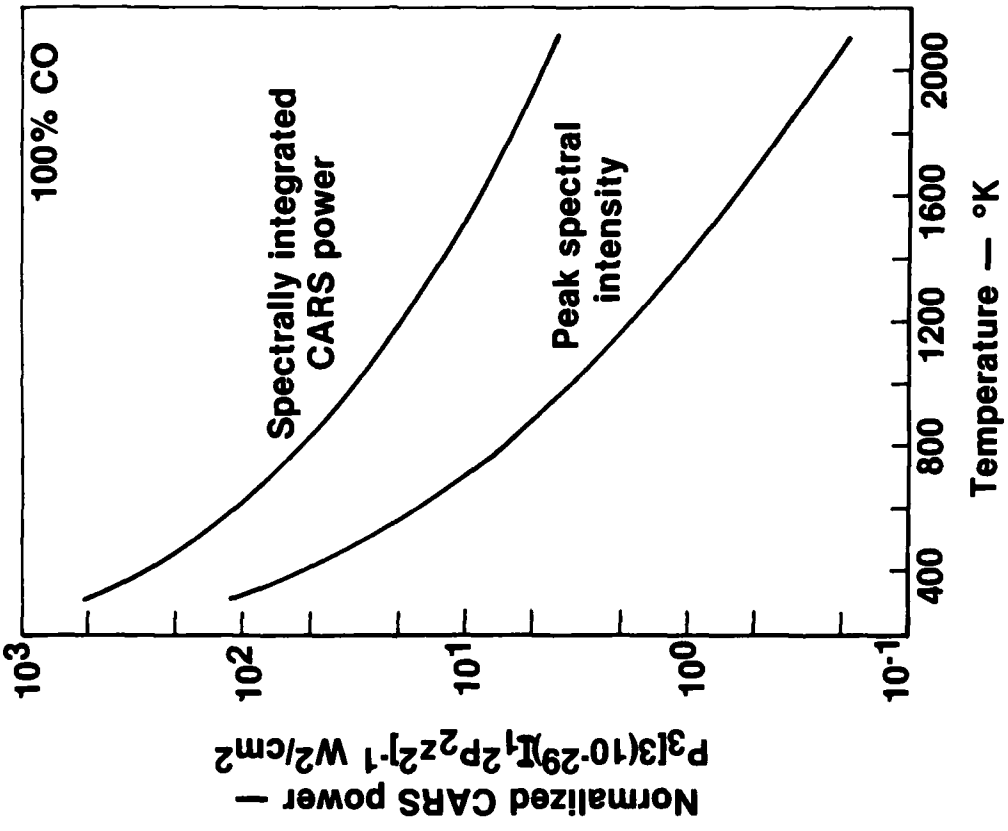

80-7-60-17

In order to ascertain whether the probe was indeed perturbing the flame, CARS measurements were made at a fixed point in the flame with the probe positioned at various locations through the flame zone. The experiment is illustrated and results of it are summarized in Fig. 15. As can be seen, depending on the position of the probe, the CARS spectral shape with aligned polarization, and thus the fractional CO concentration, changes markedly. Depending on the probe position, the concentrations measured by CARS vary between approximately 1 and 6 percent. It may not be surprising that the flame will be perturbed when the probe is near the reaction zone. Somewhat suprising is the effect of the probe even when out in the diluent shield gas zone. Thus probes with bent or hooked tips may even be questionable for use in such flames.

Calibration

Detectivity limits of CARS with and without the nonresonant susceptibility suppressed were compared using concentrations determined from the shape of CARS spectra with the background present, i.e. with aligned polarizations. These comparisons are presented in the next section. To verify the accuracy of the spectral shape approach, concentration measurements were performed over a 7.6 dia. flat flame burner and compared with the quartz microprobe reading. In this situation the microprobe should be relatively nonperturbing. Measurements were made at 300°K with the flame off and near 2100°K with the flame. To avoid the complication of the off-resonant susceptibility contribution of N_2, the detectivity limit examinations in the flat diffusion flame and, hence, the calibrations were performed with Argon diluent. The cold calibration was performed in a mixture of CO and Ar flowed through the flat flame burner. The CO concentration was sampled and measured with the Beckman Infrared Analyzer. In Fig. 16, is shown the comparison of the experimentally obtained CARS spectrum and the predicted CARS spectrum (as the overlay) for a 2.1% mixture of CO in Ar as measured with the probe sampling system. In obtaining the excellent fit in Fig. 16, the Stokes dye laser spectrum was not exactly centered on the Q-branch bandhead of CO and this was taken into account. The dye spectrum was centered at 16639 cm^{-1} and not 16654 cm^{-1} corresponding to the 2143 cm^{-1} CO Q-branch bandhead shift. The computer calculations shown in Appendix A were for the Stokes laser centered at 16667 cm^{-1} midway between the $v = 0 \rightarrow 1$ and $v = 1 \rightarrow 2$ bandheads. From the computer calculations in Appendix A which display the concentration variation of the CARS spectral shape, together with the excellent agreement displayed in Fig. 16, it is clear that accurate concentration measurements can be made from CARS spectral shapes. Measurements probably can be made to within $\pm$ 10% accuracy.

The high temperature calibration was performed in the post flame region of the aformentioned burner with an initial gas mixture of Ar, CO, CH_4 and O_2. Figure 17 displays the experimental CARS signature and the theoretical CARS overlay at a CO concentration of 3.6% measured with the quartz microprobe sampling system. Because of the high temperature, the measurement signal/noise is lower than in Fig. 16. The CARS spectrum was averaged over approximately 500 laser pulses, or 50 seconds. As in earlier examples, the noise arises from the quantum statistical uncertainty in the subtraction of the OMA tube dark current. Nevertheless the agreement between the CARS and probe measurements is again quite good.

PROBE PERTURBATION IN FLAT DIFFUSION FLAME

Folded BOXCARS at X = − 6mm; CO-air-Ar flame; splitter plate at X = 0; aligned polarizations

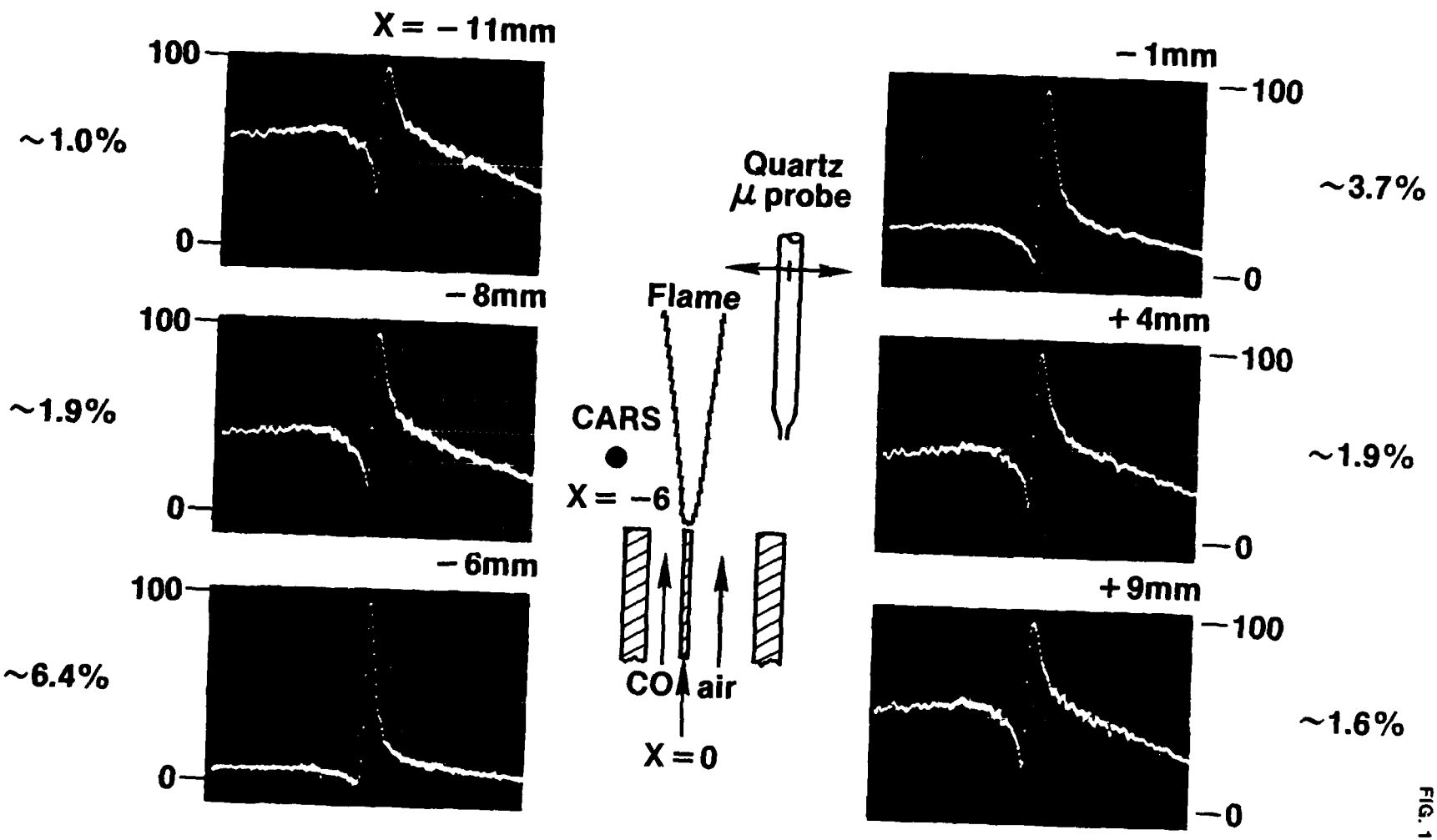

80-7-60-7

FIG. 15

COLD GAS MIXTURE CARS CALIBRATION

Measured CO concentration (ndir) 2.1% in Argon; T = 300°K;
thin solid line — CARS theory at same concentration

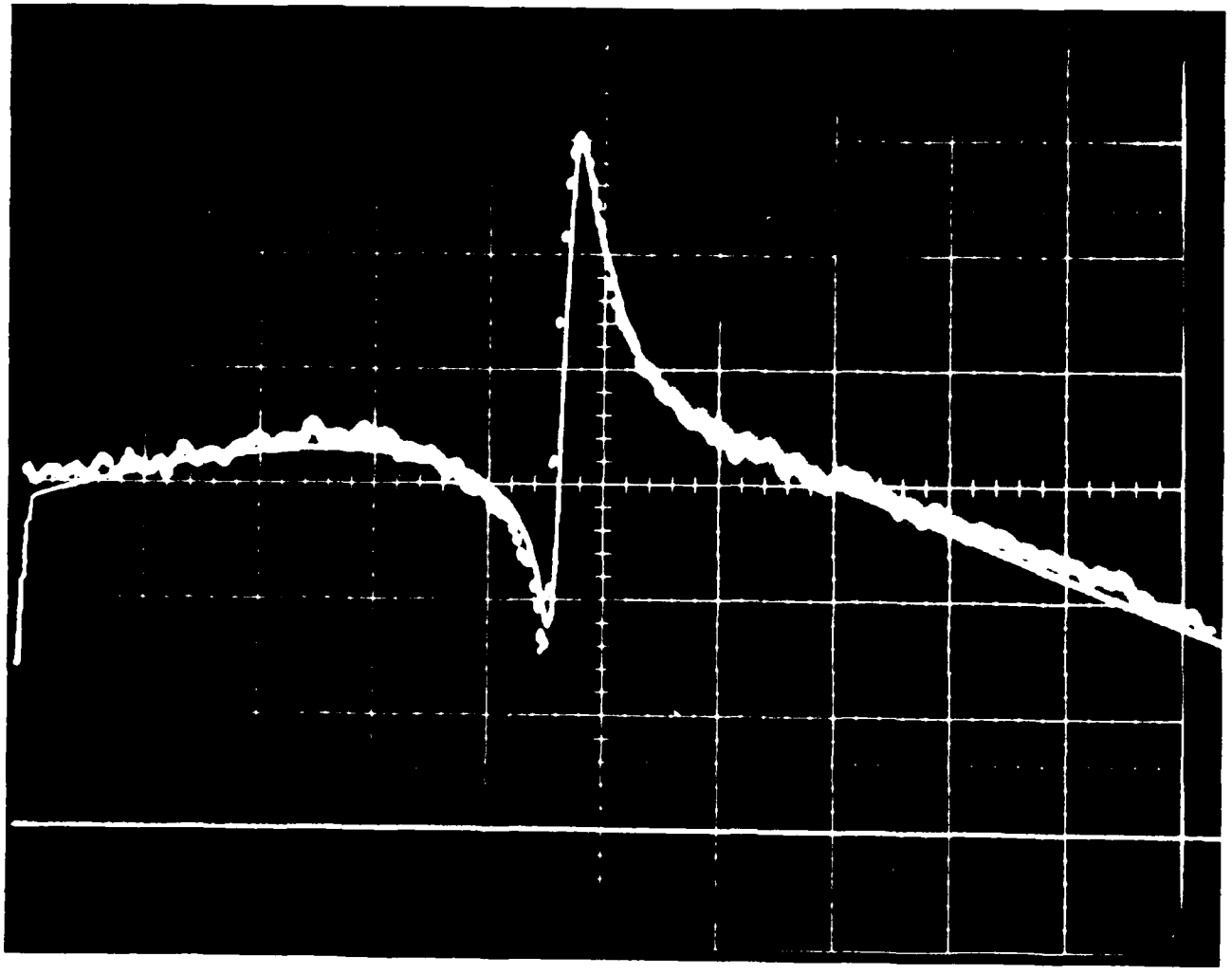

FIG. 16

CARS CONCENTRATION MEASUREMENT CALIBRATION IN A PREMIXED FLAT FLAME

Measured CO concentration (ndir) — 3.6%; thin solid line — CARS theory at same concentration and 2100°K

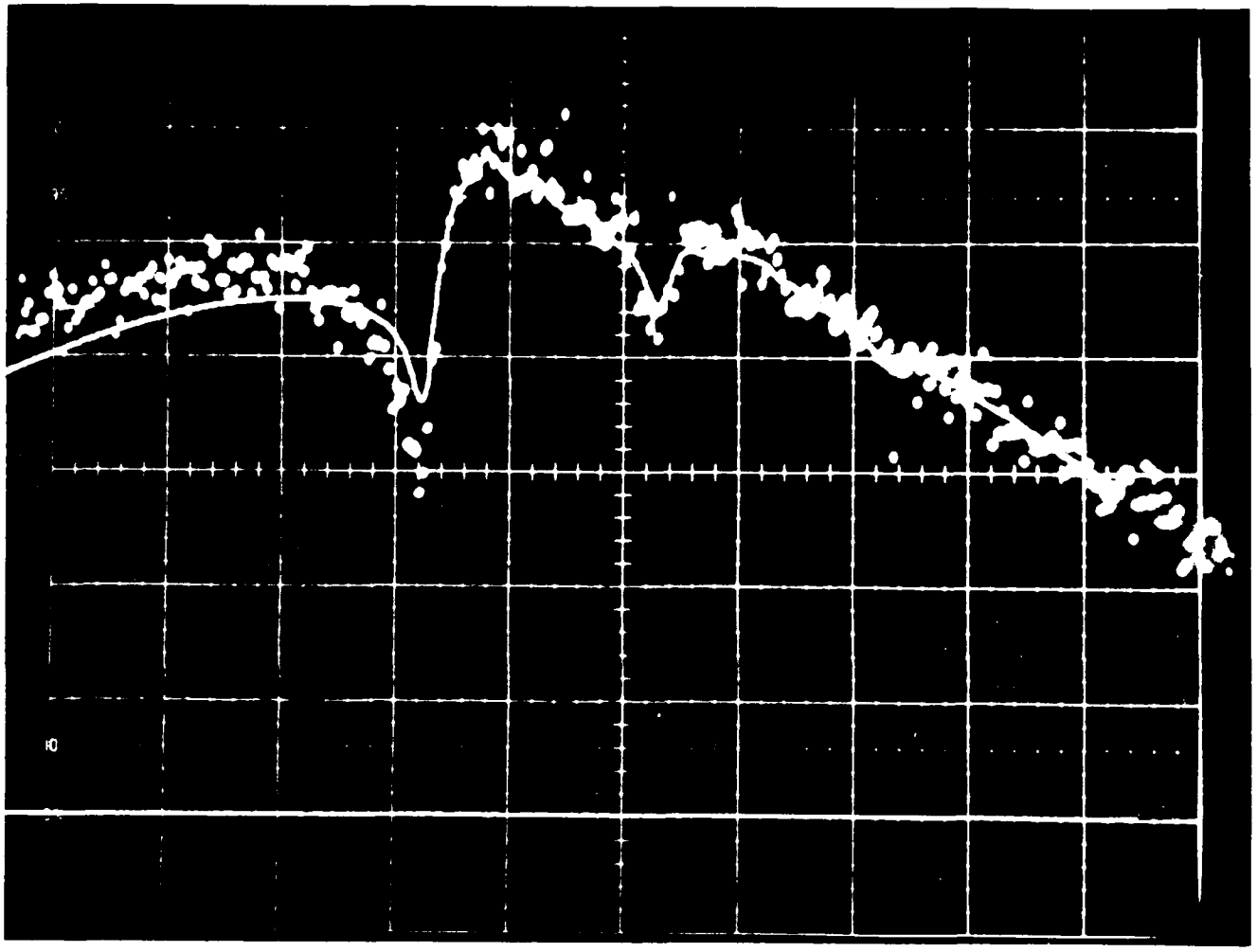

80-7-60-16

FIG. 17

Detectivity Limit Comparisons

CO spectra were recorded with and without the nonresonant susceptibility suppressed to examine the relative detectivity limits of the two approaches. The examinations were conducted in both the high and low temperature regions of the flat diffusion flame. On the cold side, the CO level decays as the CO diffuses into the diluent shield gas. On the hot or flame side, the CO and air diffuse together and react leading to the loss of CO. Due to the sensitive nature of the flat flame, measurements with and without background were made sequentially at each location in the flame to assure a valid comparison before moving on to a new location. This precaution may not have been absolutely necessary; data taken over a several week period of time were fairly consistent and reproducible. All of the results to be presented here were taken with Argon as the diluent shield gas and with the angles $\theta = \phi = 60^{o}$, $\alpha = 120^{o}$ when the background was suppressed.

In Fig. 18 the cold side detectivity comparisons are displayed. With the nonresonant susceptibility suppressed, the detectivity limit is imposed by signal photon level considerations. In the case here, detectivity is not quantum limited but is degraded slightly by the optical multichannel detector dark current. The detectivity limit with background suppressed is approximately 0.5% as seen which is ascertained from the spectrum with aligned polarizations, i.e. with the nonresonant susceptibility present. With the nonresonant susceptibility present, the detectivity is ultimately limited by the loss of modulation in the nonresonant background CARS spectrum. Although not shown in Fig. 18, modulations down to 10%, i.e. a 10% dip in the nonresonant background level, were easily recorded corresponding to a concentration level of 0.2%. It is estimated that modulations of five percent could also be seen for a cold side detectivity limit of 0.1%, approximately five times better than with the nonresonant susceptibility suppressed.

In Fig. 19 detectivity comparisons in the flame are presented with and without the background present. In both cases now, the detectivity becomes limited at the photon count level comparable to the statistical uncertainty in the dark current subtraction. With the background suppressed, the detection limit was approximately 10% at a temperature of approximately $2000^{o}K$. It should also be noted that the experimentally obtained count levels are within an order of magnitude of those that would be expected on the basis of the Fig. 14 calculations and the experimental parameters employed. With the nonresonant susceptibility present, the detectivity was again better as indicated in Fig. 20 where the CO concentration could be tracked farther into the reaction zone. The S/N limited the CARS sensitivity with aligned polarizations to about the 1-2 percent level. In actuality, the detectivitv would be somewhat better considering the four to one s/p polarization efficiency exhibited by the holographic grating in the Czerny-Turner spectrograph. These detectivity levels with the nonresonant background present are comparable to the sensitivity limits calculated in Ref. 49 for background-free CARS and a narrowband Stokes laser. There a 2% CARS sensitivity limit for CO was calculated for an atmospheric pressure, $2000^{o}K$ flame. A one second measurement time, corresponding to an average over ten pulses, was assumed, but measurements were restricted to a

COLD CO DETECTIVITY W/WO BACKGROUND SUSCEPTIBILITY SUPPRESSION

Folded BOXCARS in a CO-air-Ar flat diffusion flame;
cancellation ω_1, ω'_1 (60°): ω_2(0°): ω_3(120°)
30 second averages

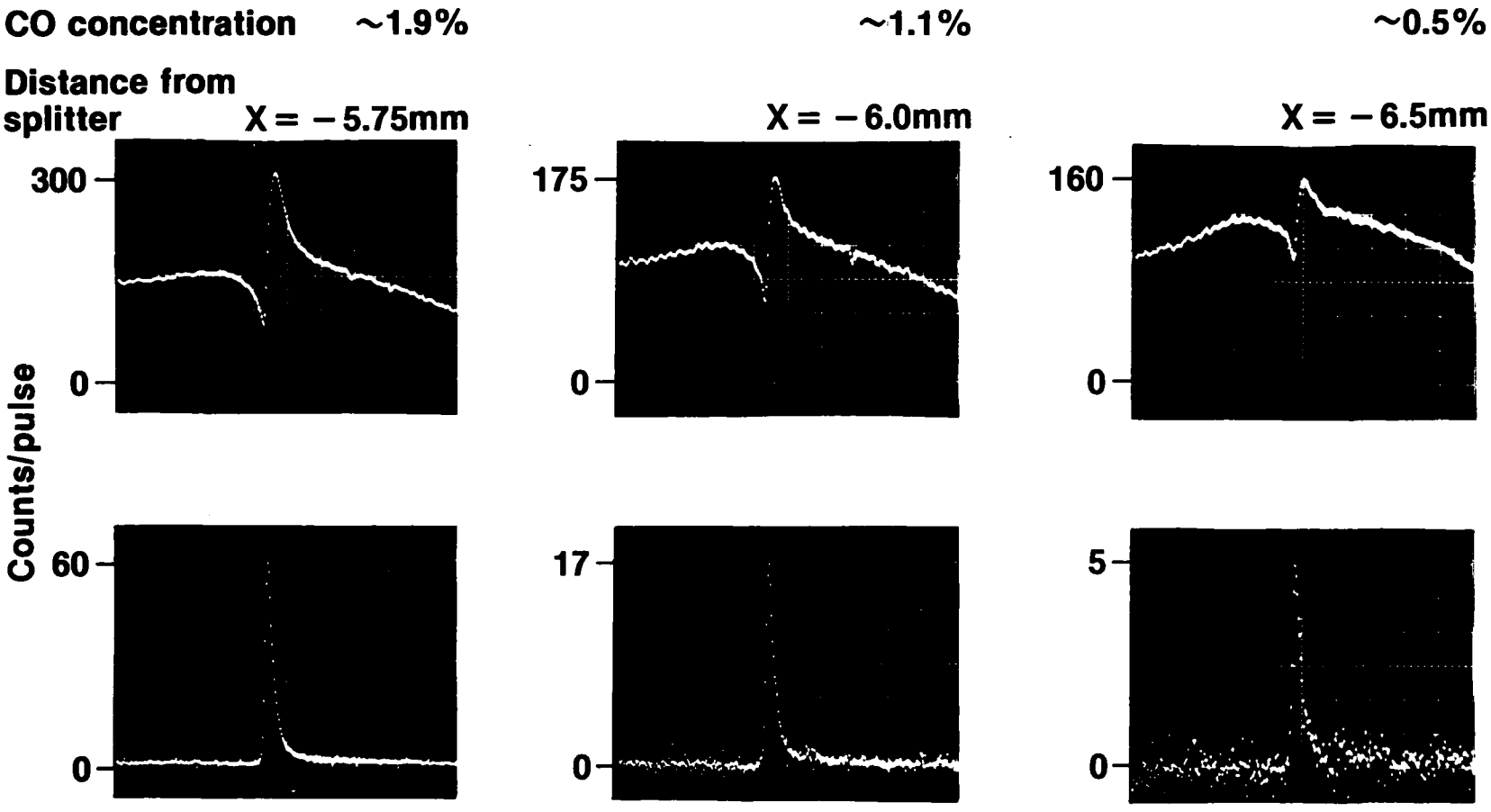

FIG. 18

80-7-60-6

FLAME CO DETECTIVITY COMPARISON W/WO NONRESONANT BACKGROUND

Folded BOXCARS in a flat CO-air-Ar flame; cancellation ω_1, $\omega_1'(60°)$: $\omega_2(0°)$: $\omega_3(120°)$

$T \approx 2000°K$ 30 second averages

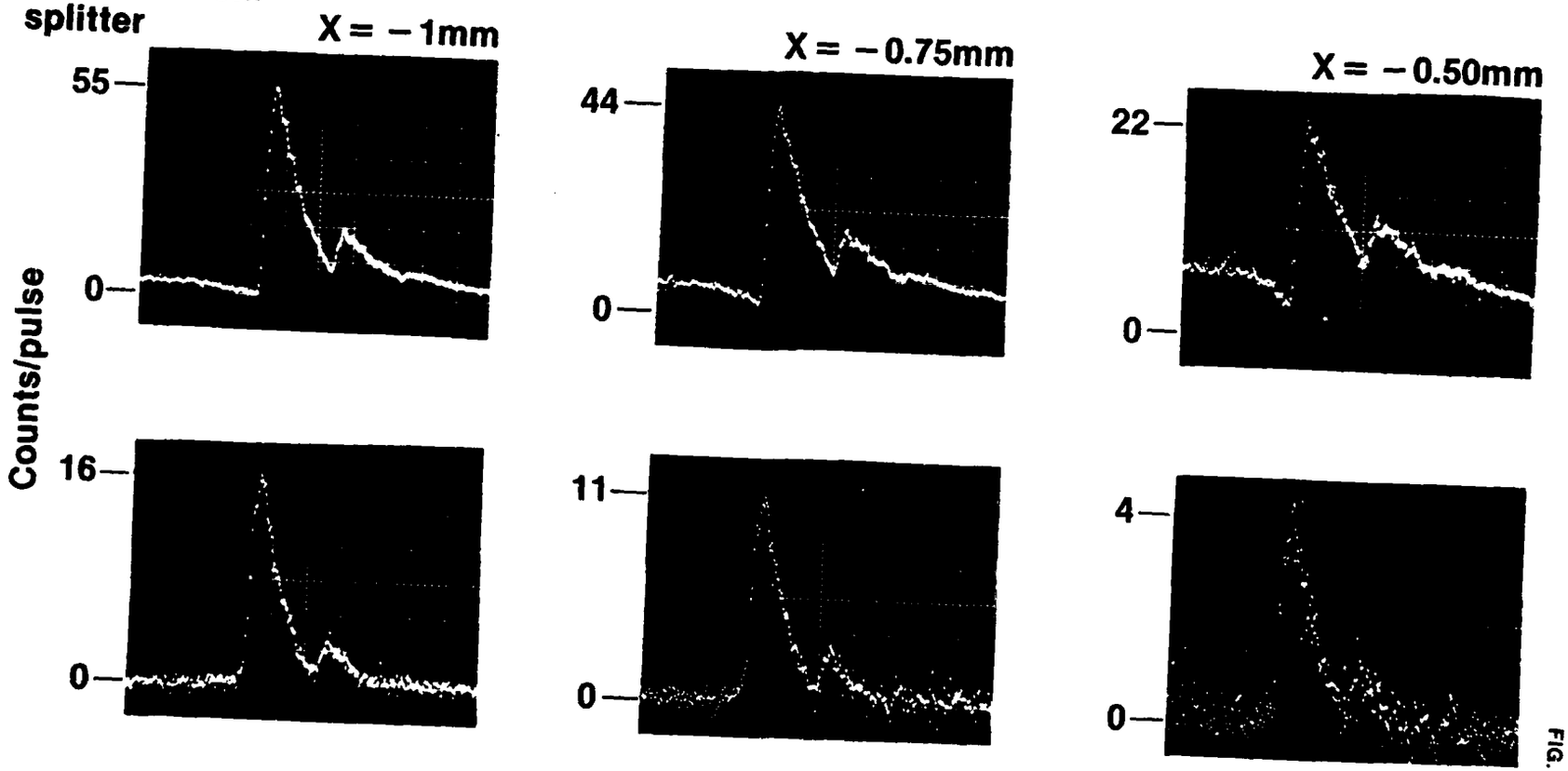

FIG. 19

FLAME CO DETECTIVITY WITH NONRESONANT BACKGROUND

Folded BOXCARS in a flat CO-air-Ar flame

T≈2000°K

30 second averages

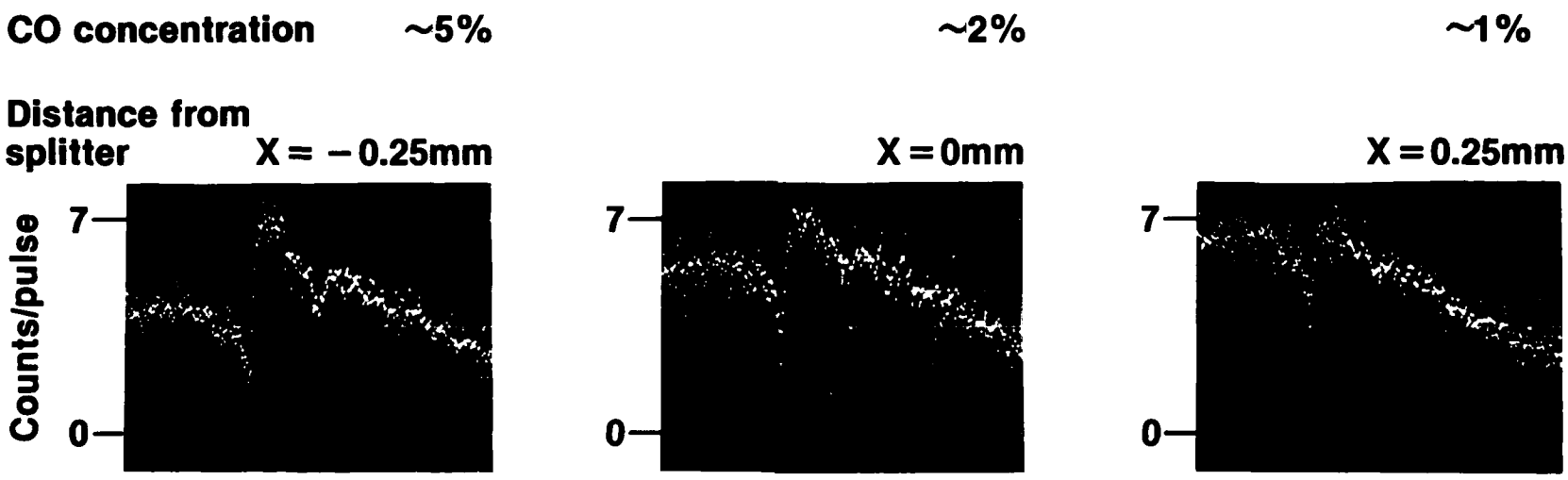

80-7-60-8

FIG. 20

single Q-branch transition. Temperature measurements would need to be made separately in order to reduce the intensity data to obtain concentration levels. Here, in the broadband case, although longer measurement times were employed, the entire spectrum is recorded and temperature can be obtained from the same spectrum. Furthermore, since concentration is derived from the spectral shape, reference cells are not required as would be in the background free case.

DISCUSSION AND CONCLUSIONS

With the nonresonant susceptibility suppressed or cancelled, density/concentration measurements are based upon the intensity of the spectrally-integrated CARS signature (Ref. 50). This necessitates the use of a reference cell to normalize for pulse-to-pulse laser power fluctuations, to serve as a calibrating standard, and to account for small optical misalignments. The latter can be accomplished only if the CARS signals from the test region and reference cell respond to optical misalignment in exactly the same manner, which, experimentally, requires some care to achieve. Even with a normalizing reference cell and a single mode pump laser, normalized CARS signals are subject to fluctuations on the order of 5-7% even from a quiescent gas (Ref. 51). In practical combustion systems, serious problems confront CARS density measurements made from spectrally-integrated intensity levels. Beam attenuation from soot and/or fuel droplets together with turbulence-induced steering and defocussing, which degrade the efficiency of CARS generation, must be accounted for in some manner. One approach, although not exact, would be to employ reference cells both before and after the test region, clearly at the expense of experimental complexity. Even in this case, it is probably not possible to distinguish between a signal decrease due to a parameter fluctuation from that due to attenuation, or that due to refractive index nonuniformities leading to an ambiguity in how to "correct" the raw data. Signal reductions due to attenuation are potentially correctable if beam transmission is monitored in some manner and accounted for. In the case of turbulence-induced signal decreases, i.e. due to beam steering and defocussing, a post-measurement-volume reference cell would indicate that the CARS generation process was perturbed. It would be difficult, however, to account and correct for such effects in a rigorous, quantitative manner.

In light of the above, together with the higher CARS detection sensitivity with aligned polarizations, it seems extremely attractive therefore, to perform concentration measurements from spectral shapes whenever possible and to explore means which extend the range over which such an approach is applicable. When using spectral shapes to perform measurements, extinction effects due to soot and/or droplets and refractive effects are unimportant as long as the signal is acquirable with good photon statistics. In essence one employs the background nonresonant susceptibility as an in-situ calibrating standard. As mentioned earlier, for air-fed combustion processes, the susceptibility undergoes relatively minor variations in the composition change accompanying the transition from reactants to products. For example, in methane-air combustion, the density-normalized nonresonant susceptibility increases by about 14% between the reactants and products. Based upon the measured temperature and/or location in the combustor, intelligent estimates can be made of the nonresonant susceptibility value best employed to minimize the measurement uncertainty. It is speculated here that this is a more attractive approach, in terms of both simplicity and ultimate accuracy, for concentration determinations than the use of spectrally-integrated intensity measurements employing reference cells. Aside from practical combustor measurements, it may be possible to configure fundamental turbulent combustion experiments to minimize the reactant to product variation in the background susceptibility. This

can be achieved by using excess N_2 as diluent or substituting a diluent with a higher background susceptibility than N_2, e.g. CO_2. This is analogous to the composition tailoring used in Rayleigh scattering diagnostics to achieve a nearly composition independent, total Rayleigh cross section (Ref. 52).

For most molecules of combustion interest, with the exception of H_2, the nominal range for concentration measurements from spectral shapes, exploiting the interference with the nonresonant susceptibility, is between 0.1% to 10-20% for aligned polarizations. Polarization orientation may be employed to extend this range. At the lower end, the polarizations of the incident waves may be oriented to reduce the background level not totally,but in steps, e.g. by factors of two, four etc. Furthermore, this can be achieved without incurring as large a resonant mode signal penalty as encountered with complete cancellation. To extend the upper range, polarization orientation can be used to reduce the resonant contribution relative to the nonresonant background to create or enhance the interference. In the upper ranges the interference exists, but is generally not large and, hence is not detected when examining the squared modulus of the susceptibility with optical multichannel detectors of limited dynamic range.

A better idea, perhaps, for measurements at high concentrations has been proposed by Ultee (Ref. 53). For background-free CARS spectra, i.e. high species concentrations or low concentrations with the nonresonant susceptibility suppressed, the nonresonant susceptibility at the measurement location is employed as an in-situ reference in a slightly different manner. In addition to the normal broad-band Stokes wave centered on or near the species resonance of interest, a second, but narrowband, Stokes beam would be employed as illustrated in Fig. 21. This would be tuned considerably off the high frequency side of the resonant bandhead to generate a reference signal level from the background susceptibility. Both Stokes beams could be generated from the same dye laser using an intra-cavity polarization splitter (Ref. 54). The nonresonant CARS reference and resonant CARS signal beams would be recorded simultaneously within the spectral field of the optical multichannel detector. Temperature would be ascertained from the shape of the resonant CARS signature as usual. The total gas density would follow from the gas law knowing the pressure which would thus calibrate the nonresonant CARS reference. The concentration of the resonant species would be determined by comparison with the strength of the nonresonant reference. Such a measurement approach would be immune to medium extinction and refraction effects since all beams would be similarly affected.

IN-SITU NONRESONANT SUSCEPTIBILITY REFERENCE CONCEPT FOR CARS DENSITY MEASUREMENTS

a) Two wavelength dye laser

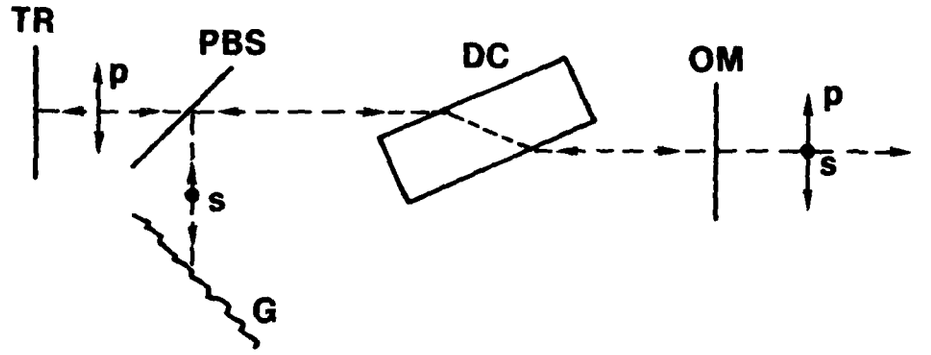

b) Spectrum

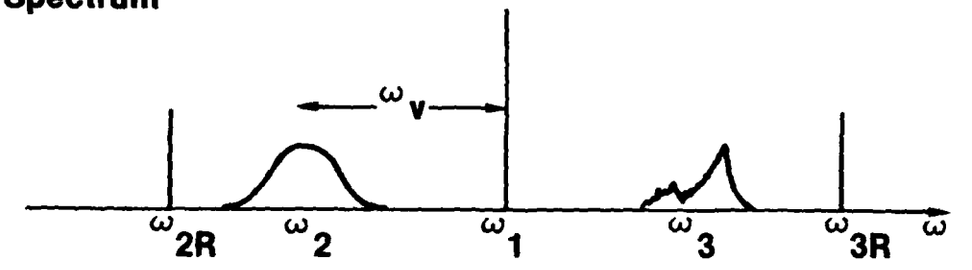

FIG. 21

REFERENCES

1. Nibler, J. W., W. M. Shaub, J. R. McDonald, and A. B. Harvey: Coherent Anti-Stokes Raman Spectroscopy. in Vol. 6, Vibrational Spectra and Structure, J. R. Durig, Ed. Elsevier, Amsterdam, 1977.

2. Eckbreth, A. C., P. A. Bonczyk and J. F. Verdieck: Combustion Diagnostics by Laser Raman and Fluorescence Techniques. Prog. Energy Combust. Sci., Vol. 5, pp. 253-322, 1979.

3. Druet, S. and J. P. Taran: Coherent Anti-Stokes Raman Spectroscopy. in Chemical and Biological Application of Lasers, C. B. Moore, Ed., Academic Press, New York, 1979.

4. Nibler, J. W. and G. V. Knighten: Coherent Anti-Stokes Raman Spectroscopy. in Vol. II, Topics in Current Physics, A. Weber, Ed., Springer-Verlag, Heidelberg, 1979.

5. Lapp, M. and C. M. Penney: Laser Raman Gas Diagnostics. Plenum Press, New York, 1974.

6. Lederman, S.: The Use of Laser Raman Diagnostics in Flow Fields and Combustion. Prog. Energy Combust. Sci., Vol. 3, pp. 1-34, 1977.

7. Zinn, B. T. (Ed.): Experimental Diagnostics in Gas Phase Combustion Systems. AIAA, New York, 1977.

8. Lapp, M. and D. L. Hartley: Raman Scattering Studies of Combustion. Combust. Sci. Technol., Vol. 13, pp. 199-210, 1976.

9. Roquemore, W. M. and P. P. Yaney: Comparison of Thermocouple, Gas Sampling, and Raman Measured Temperatures in an Afterburning Turbojet Engine Plume. Proceedings, NBS Tenth Materials Research Symposium on Characterization of High Temperature Vapors and Gases, pp. 973-1025, 1978.

10. Williams, W. D., H. M. Power, R. L. McGuire, J. H. Jones, L. L. Price and J. W. L. Lewis: Laser Raman Diagnostics of Temperature and Number Density in the Mixing Region of a Rocket Engine Exhaust and a Coflowing Air Stream. AIAA Paper 77-211, 1977.

11. Smith, J. R.: Time Resolved Raman Spectroscopy in a Stratified Charge Engine. Sandia Laboratories Report SAND 79-8693, 1979.

12. Setchell, R. E.: Initial Measurements Within an Internal Combustion Engine Using Raman Spectroscopy. Sandia Laboratories Report SAND 78-1220, 1978.

13. Bailly, R., M. Pealat and J. P. E. Taran: Raman Investigation of Subsonic Jet. Opt. Comm., Vol. 17, pp. 68-73, 1976.

14. Aeschliman, D. P. and R. E. Setchell: Fluorescence Limitations to Combustion Studies Using Raman Spectroscopy. Appl. Spect., Vol. 29, pp. 426-429, 1975.

15. Leonard, D. A.: Field Tests of a Laser Raman Measurement System for Aircraft Engine Exhaust Emissions. AFAPL-TR-74-100, 1974.

16. Yaney, P. P.: Combustion Diagnostics Using Laser Spontaneous-Raman Scattering. AFAPL-TR-79-2035, 1979.

17. Eckbreth, A. C.: Effects of Laser-Modulated Particulate Incandescence on Raman Scattering Diagnostics. J. Appl. Phys., Vol. 48, pp. 4473-4479, 1977.

18. Pealat, M., R. Bailly and J.P.E. Taran: Real Time Study of Turbulence in Flames by Raman Scattering. Opt. Comm., Vol. 22, pp. 91-94, 1977.

19. Eckbreth, A. C.: Applicability of Laser Raman Scattering Diagnostic Techniques to Practical Combustion Systems. Project SQUID Technical Report UTRC-4-PU, 1976.

20. Eckbreth, A. C.: CARS Investigations in Sooting and Turbulent Flames. Project SQUID Report UTRC-5-PU, 1979.

21. Eckbreth, A. C. and R. J. Hall: CARS Thermometry in a Sooting Flame. Combust. Flame, Vol. 35, pp. 87-98, 1979.

22. Attal, B.,M. Pealat and J. P. E. Taran: CARS Diagnostics of Combustion. AIAA Paper No. 80-0282, 1980.

23. Switzer, G. L., W. M. Roquemore, R. P. Bradley, P. W. Schreiber and W. B. Roh: CARS Measurements in a Bluff-Body Stabilized Diffusion Flame. Appl. Opt., Vol. 18, pp. 2343-2345, 1979.

24. Eckbreth, A. C.: CARS Thermometry in Practical Combustors. Combust. Flame, 1980. see also, Eckbreth, A. C., P. A. Bonczyk and J. F. Verdieck: Investigation of CARS and Laser-induced Saturated Fluorescence for Practical Combustion Diagnosis. EPA-600/7-80-091, 1980.

25. Stenhouse, I. A., D. R. Williams, J. B. Cole and M. D. Swords: CARS in an Internal Combustion Engine. Appl. Opt., Vol. 18, pp. 3819-3825, 1979.

26. Song, J. J., G. L. Eesley and M. D. Levenson: Background Suppression in Coherent Raman Spectroscopy. Appl. Phys. Letts., Vol. 29, pp. 567-569, 1976.

27. Akhmanov, S. A., A. F. Bunkin, S. G. Ivanov, and N. I. Koroteev: Polarization Active Raman Spectroscopy and Coherent Raman Ellipsometry. Sov. Phys. JETP, Vol. 47, pp. 667-678, 1978.

28. Bunkin, A. F., S. G. Ivanov and N. I. Koroteev: Gas Analysis by Coherent Active Raman Spectroscopy with Polarization Discrimination. Sov. Tech. Phys. Lett., Vol. 3, pp. 182-184, 1977.

29. Rahn, L. A., L. J. Zych and P. L. Mattern: Background-Free CARS Studies of Carbon Monoxide in a Flame. Opt. Comm., Vol. 39, pp. 249-253, 1979.

30. Farrow, R. L., P. L. Mattern and L. A. Rahn: Crossed-Beam, Background Free CARS Measurements in a Methane Diffusion Flame. Sandia Laboratories Report SAND 80-8640, 1980.

31. Oudar, J. L., R. W. Smith and Y. R. Shen: Polarization-Sensitivie Coherent Anti-Stokes Raman Spectroscopy. Appl. Phys. Letts., Vol. 34, pp. 758-760, 1979.

32. Kamga, F. M. and M. G. Sceats: Pulse-Sequenced Coherent Anti-Stokes Raman Scattering Spectroscopy: A Method for Suppression of the Nonresonant Background. Opt. Lett., Vol. 5, pp. 126-128, 1980.

33. Roh, W. B., P. W. Schreiber and J. P. E. Taran: Single-Pulse Coherent Anti-Stokes Raman Scattering. Appl. Phys. Letts., Vol. 29, pp. 174-176, 1976

34. Eckbreth, A. C.: BOXCARS: Crossed-Beam Phase-Matched CARS Generation in Gases. Appl. Phys. Letts., Vol. 32, pp. 421-423, 1978.

35. Laufer, G. and R. B. Miles: Angularly Resolved Coherent Raman Scattering. Opt. Comm., Vol. 28, pp. 250-254, 1979.

36. Compaan, A. and S. Chandra: Coherent Anti-Stokes Raman Scattering with Counter-propagating Laser Beams, Opt. Letts., Vol. 4, pp. 170-172, 1979.

37. Marko, K. A. and L. Rimai: Space-and Time-Resolved Coherent Anti-Stokes Raman Spectroscopy for Combustion Diagnostics. Opt. Lett., Vol. 4, pp. 211-213, 1979.

38. Shirley, J. A., R. J. Hall and A. C. Eckbreth: Rotational Raman Studies Using Folded BOXCARS. accepted for publication in Optics Letters, September , 1980.

39. Prior, Y.: Three-Dimensional Phase Matching in Four-Wave Mixing. Appl. Opt., Vol. 19, pp. 1741-1743, 1980.

40. Hall, R. J.: CARS Spectra of Combustion Gases. Combust. Flame, Vol. 35, pp. 47-60, 1979.

41. Hall, R. J., J. A. Shirley and A. C. Eckbreth: Coherent Anti-Stokes Raman Spectroscopy, Spectra of Water Vapor in Flames. Opt. Lett., Vol. 4, pp. 87-89, 1979.

42. Rado, W. G.: The Nonlinear Third Order Dielectric Susceptibility Coefficients of Gases and Optical Third Harmonic Generation. Appl. Phys. Letts., Vol. 11, pp. 123-125, 1967.

43. Lotem, H., R. T. Lynch, Jr. and N. Bloembergen: Interference between Raman Resonances in Four Wave Difference Mixing. Phys. Rev. A, Vol. 14, pp. 1748-1755, 1976 .

44. Attal, B., O. O. Schnepp and J. P. E. Taran: Resonant CARS in I_2 Vapor. Opt. Comm., Vol. 24, pp. 77-82, 1978.

45. Molectron Corporation Applications Note 112: Coherent Anti-Stokes Raman Spectroscopy (CARS) - Update. 1976.

46. Owyoung, A.: The Origins of the Nonlinear Refractive Indices of Liquids and Gases. AFOSR-TR-71-3132, 1971.

47. Exciton Chemical Company, Dayton, Ohio 45431.

48. Wolfhard, H. G. and W. G. Parker: A New Technique for the Spectroscopic Examination of Flames at Normal Pressures. Proc. Phys. Soc. A, Vol. 62, pp. 722-730, 1949.

49 Rahn, L. A., P. L. Mattern and R. L. Farrow: A Comparison of Coherent and Spontaneous Raman Combustion Diagnostics. Sandia Laboratories Report SAND 80-8616, June 1980.

50. Roh, W. B. and P. W. Schreiber: Pressure Dependence Of Integrated CARS Power. Appl. Opt., Vol. 17, pp. 1418-1424, 1978.

51. Taran, J. P. E., ONERA, Chatillon, France. private communication.

52. Rambach, G. D., R. W. Dibble and R. E. Hollenback: Velocity and Temperature Measurements in Turbulent Diffusion Flames. Western States Section Combustion Institute Paper 79-51, 1979.

53. Ultee, C. J., United Technologies Research Center, East Hartford, Connecticut, 06108. private communication.

54. Piloff, H. S.: Simultaneous Two-Wavelength Selection in the N_2 Laser-Pump Dye Laser. Appl. Phys. Letts., Vol. 21, pp. 339-340, 1972.

APPENDIX A

CONCENTRATION SENSITIVITY OF CARS SPECTRA WITH NONRESONANT BACKGROUND SUSCEPTIBILITY

The ability to perform CARS concentration measurements without nonresonant background suppression depends critically on the value of the background susceptibility employed in the computer simulations (Ref. A-1). At low CO concentrations, the inferred CO number density will be directly proportional to the value of the background susceptibility used in the computer fitting. This procedure is capable of high accuracy if the nonlinear background is known.

Rado (Ref. A-2) has reported values of χ^{nr} for many gases of interest. DeMartini, et.al. (Ref. A-3) have confirmed the Rado measurements for N_2 and O_2, although they did obtain a value of χ^{nr} for He about a factor of four larger than Rado's value. The latter discrepancy may be due to the smallness of the He susceptibility. It must be noted however, that the Rado and DeMartini experiments did not measure absolute values for the susceptibilities, but rather values normalized to an assumed number of $\chi^{(3)}$ for the Q(1) line of H_2 on resonance. This assumed value is 2.1×10^{-13} cm^3/erg, obtained from electric field-induced absorption measurements. For reasons that cannot be deduced from the sources cited, however, this H_2 susceptibility value is not consistent with the way in which the resonant vibrational-rotational contribution to $\chi^{(3)}$ is normally calculated (Ref. A-1). If a theoretical $\chi^{(3)}$ for H_2 Q(1) is calculated using the formulation found in Ref. A-1, the result is a number that is two to three times the Rado value, even after the Rado number has been multiplied by a factor of three to standardize the definition of $\chi^{(3)}$. The range of two to three reflects the variation in the reported values of the Q(1) spontaneous Raman cross section (Ref. A-4) and the homogeneous (pressure-broadened) linewidth (Refs. A5-A8). With regard to the susceptibility number on which the Rado-DeMartini values are based, it is possible that the field-induced absorption measurement was not accurate, or there may be an assumed convention for the susceptibility that is not explicitly stated (such as the factor of ½ convention introduced by Maker and Terhune (Ref. A-9)). It is to be noted that Rado points out that the susceptibility value he reports for Ar is about a factor of three lower than a value derived from Kerr effect data, and that the assumed H_2 susceptibility does not account for all the features of stimulated Raman scattering in H_2 (Ref. A-2).

Given these uncertainties about the number to which the Rado-DeMartini susceptibility numbers are normalized, the consistent course is to use the Refs. A-2, A-3 results for the relative contributions to χ^{nr} due to different chemical species, but to scale all the absolute magnitudes in accordance with a theoretical susceptibility value for Q(1) of H_2. If the larger of the two spontaneous Raman cross sections reported in Ref. A-4 and the linewidth value of Ref. A-8 are employed in the theoretical calculation of the H_2 susceptibility, the result is that the Rado-DeMartini susceptibility numbers should be scaled up by a factor of about 2.5. The resulting background susceptibility for Ar gives very good agreement with measurements in a calibrated CO-Ar test mixture as reported in the calibration section. In Table A-I, revised susceptibility values using the above procedure are presented for various species.

TABLE A-I

REVISED BACKGROUND SUSCEPTIBILITY VALUES*

Gas	$\chi^{nr}(x10^{18} cm^3/erg)$
He	2.78
Ar	11.63
D_2	9.75
N_2	10.13
O_2	9.75
NO	31.5
CH_4	22.13
C_2H_6	46.5
CO_2	15.0

*To be used in the following expression for $\chi^{(3)}$

$$\chi^{(3)} = \frac{2c^4}{\hbar\omega_2^4} N \sum_j \frac{\Delta_j (\partial\sigma/\partial\Omega)_j}{2\Delta\omega_j - i\Gamma_j} + \chi^{nr}$$

Using the newly calculated value for the background nonresonant susceptibility of Ar, computer calculations over a matrix of CO concentrations and gas temperatures are presented in the following pages. These calculations were used to deduce the CO concentrations reported in the body of the report. The calculations assumed the CO Raman linewidths were similar to those of N_2 and include appropriate temperature and rotational quantum number dependences (Ref. A-10). Calculations showed that the computed spectra were not very sensitive to the Raman linewidths unless extremely low values were chosen.

APPENDIX A REFERENCES

1. Hall, R. J.: CARS Spectra of Combustion Gases. Combust. Flame, Vol. 35, pp. 47-60, 1979.

2. Rado, W. G.: The Nonlinear Third Order Dielectric Susceptibility Coefficients of Gases and Optical Third Harmonic Generation. Appl.Phys. Lett., Vol. 11, pp. 123-125, 1967.

3. DeMartini, F., F. Simoni and E. Santomato: High Resolution Nonlinear Spectroscopy. Dicke Narrowing and Dispersion of the Third-Order Nonlinear Susceptibility of H_2 near the Q(1) Vibrational Resonance. Opt. Comm., Vol. 9, pp. 176-81, 1973.

4. Murphy, W. F., W. Holtzer and J. J. Bernstein: Gas Phase Raman Intensities: A Review of "Pre-Laser Data". Appl. Spect., Vol. 23, pp. 211-18, 1969.

5. Henesian, M. A., L. Kulevskii, R. L. Byer and R. L. Herbst: CW High-Resolution CARS Spectroscopy of H_2, D_2, and CH_4. Opt. Comm., Vol. 18, pp. 255-6, 1976.

6. Allin, E. J., A. D. May, B. P. Stoicheff, J. C. Stryland and H. L. Welsh: Spectroscopy Research at the McLennan Physical Laboratories of the University of Toronto. Appl. Optics, Vol. 6, pp. 1597-1608, 1967.

7. Murray, J. R. and A. Javan: Motional Narrowing in Hydrogen Raman Scattering. J. Mol. Spectry., Vol. 29, pp. 502-4, 1969.

8. Lallemand, P. and P. Simova: Stimulated Raman Spectroscopy in Hydrogen Gas. J. Mol. Spectry., Vol. 26, pp. 262-76, 1968.

9. Maker, P. D., and R. W. Terhune: Study of Optical Effects Due to an Induced Polarization Third Order in Electric Field Strength. Phys. Rev., Vol. 137, pp. A801-A818, 1965.

10. Hall, R. J.: Pressure-Broadened Linewidths for N_2 CARS Thermometry. Accepted for publication in Applied Spectroscopy, 1980.

Concentration Series

The following graphs present the temperature behavior of CO CARS spectra at a fixed concentration over the range of concentrations from 0.5 to 100.0% as noted. The temperatures employed in the calculations vary from bottom to top in 300 K increments from $300^{o}K$ to $2100^{o}K$.

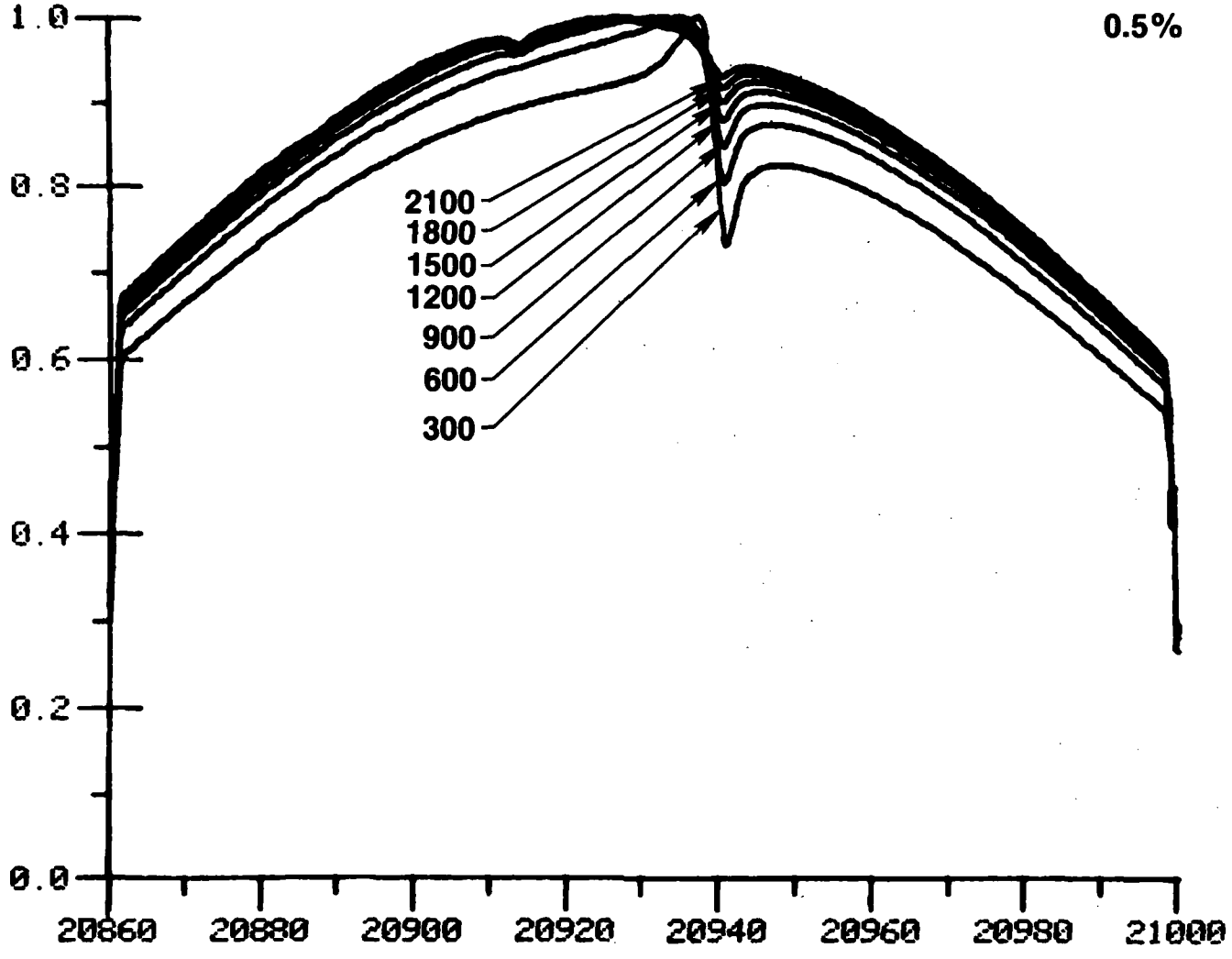
0.5%
2100
1800
1500
1200
900
600
300
1.0
0.8
0.6
0.4
0.2
0.0
20860
20880
20900
20920
20940
20960
20980
21000

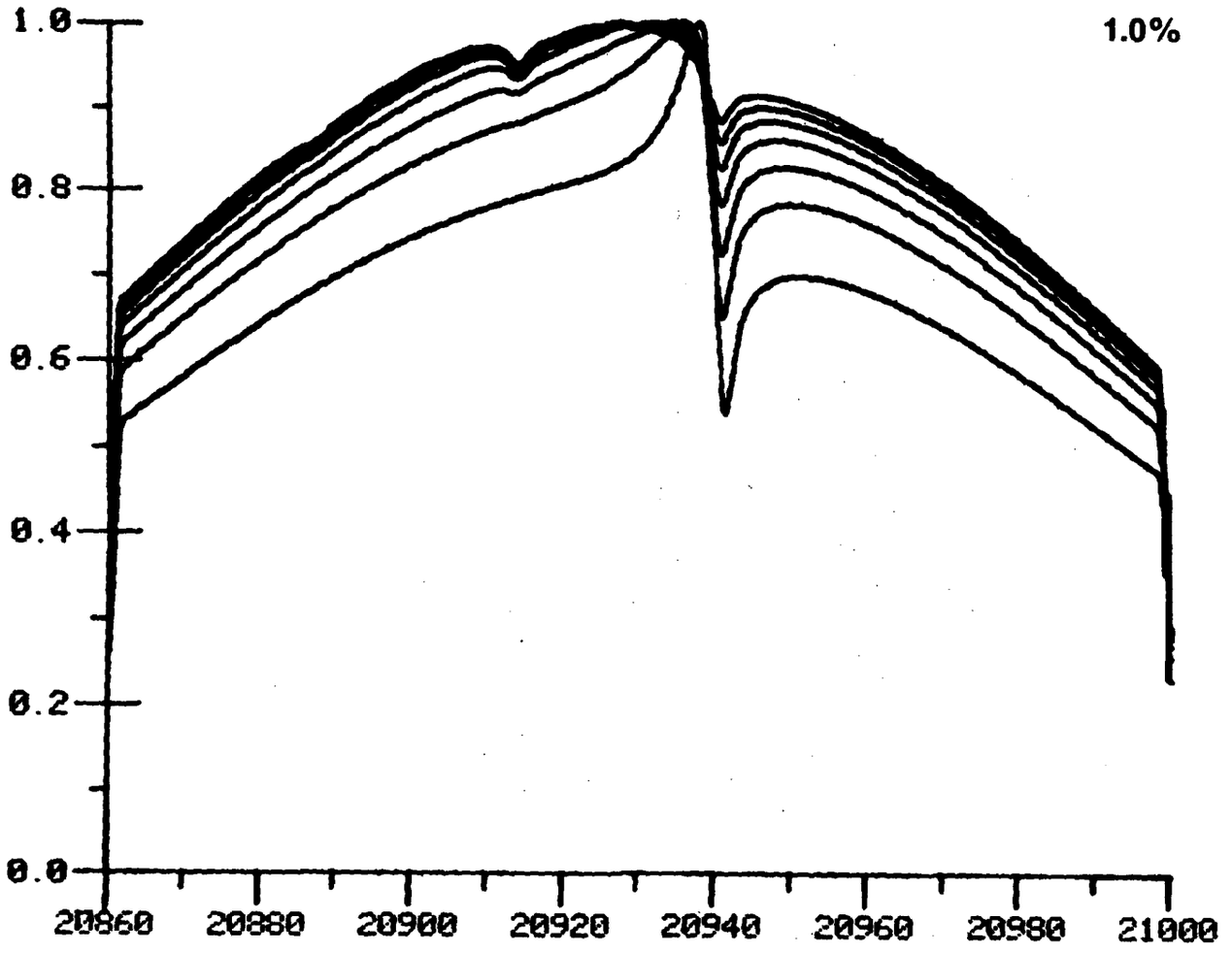
1.0%
1.0
0.8
0.6
0.4
0.2
0.0
20860
20880
20900
20920
20940
20960
20980
21000

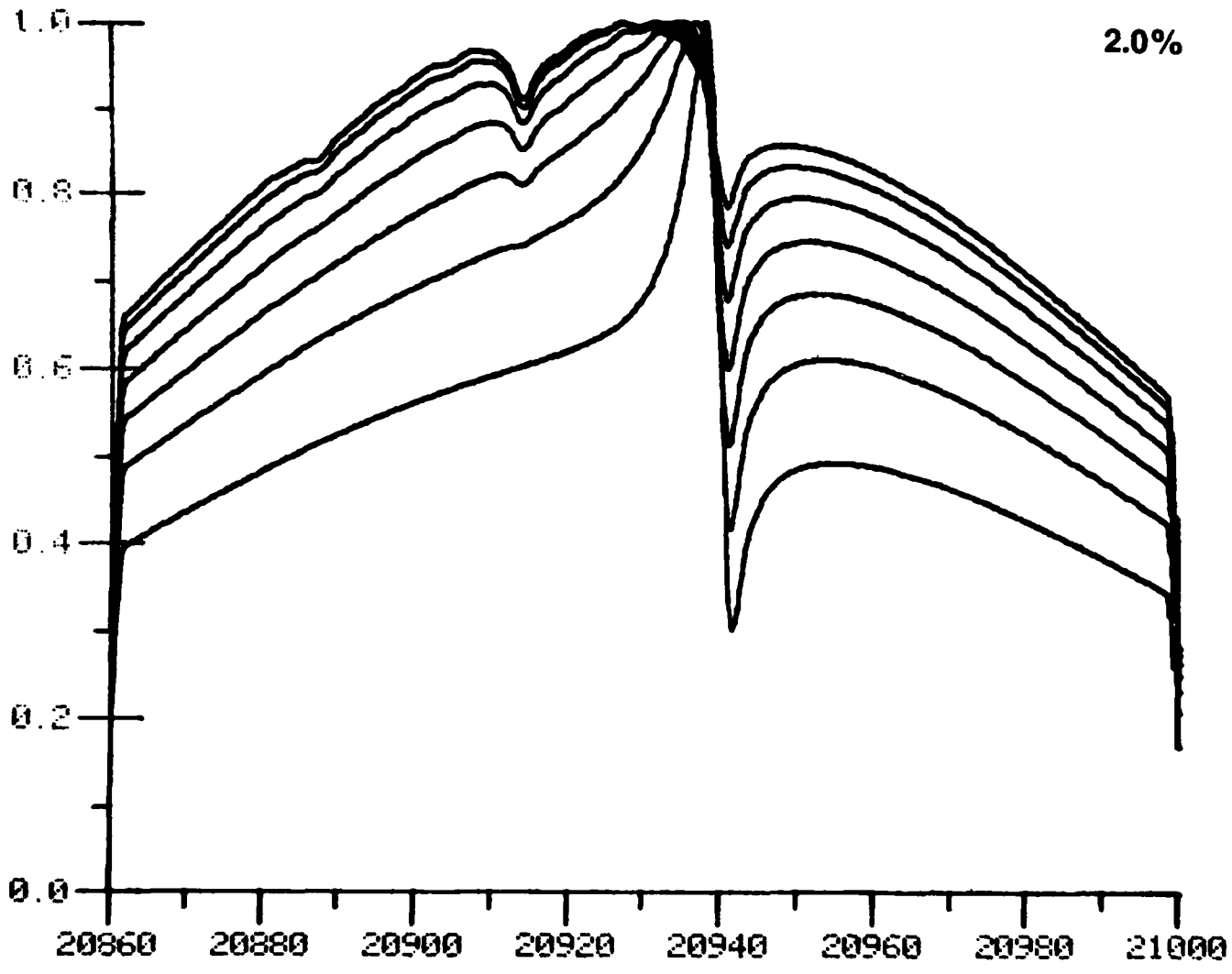
2.0%
1.0
0.8
0.6
0.4
0.2
0.0
20860
20880
20900
20920
20940
20960
20980
21000

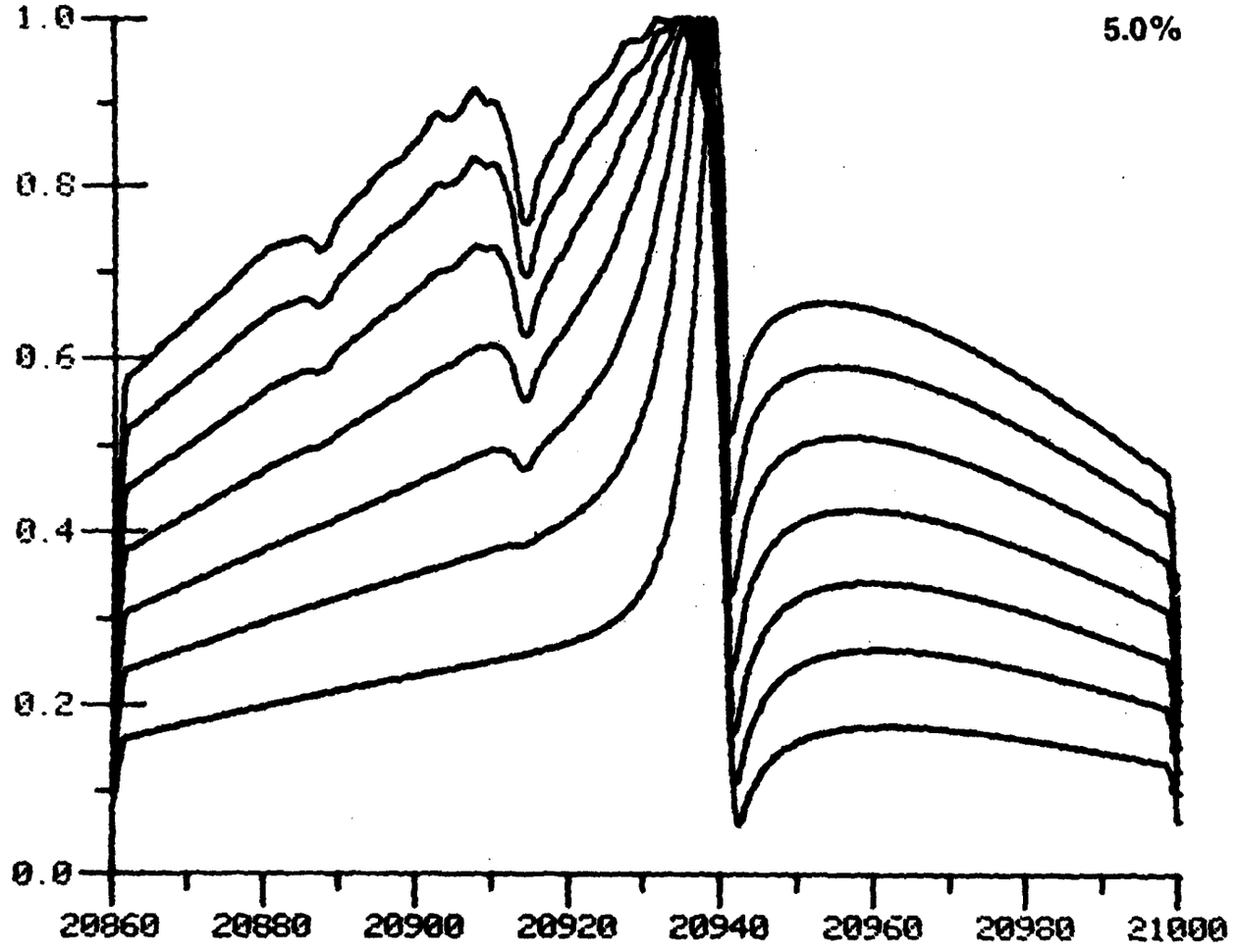
5.0%
1.0
0.8
0.6
0.4
0.2
0.0
20860
20880
20900
20920
20940
20960
20980
21000

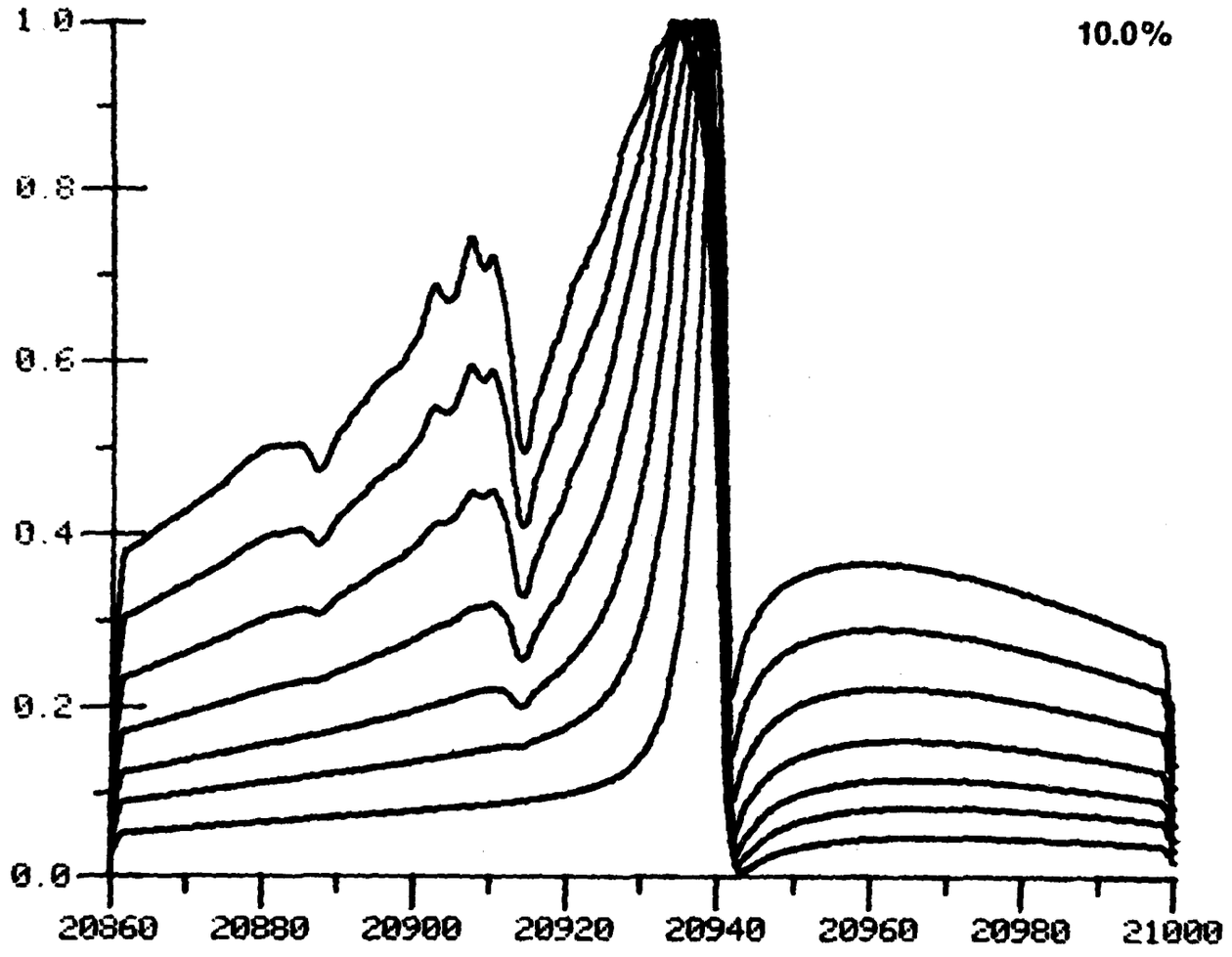
10.0%
1.0
0.8
0.6
0.4
0.2
0.0
20860
20880
20900
20920
20940
20960
20980
21000

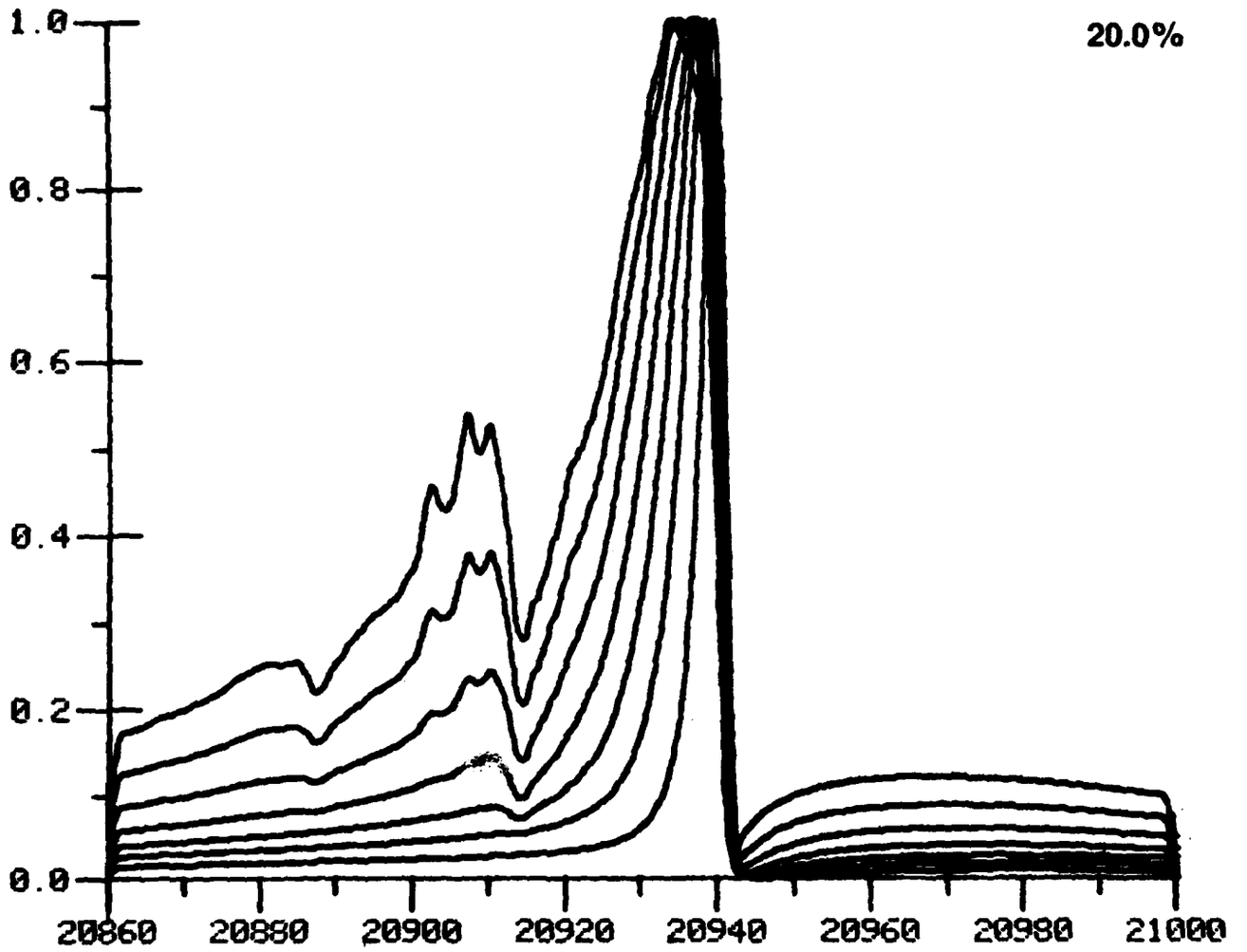
20.0%
1.0
0.8
0.6
0.4
0.2
0.0
20860
20880
20900
20920
20940
20960
20980
21000

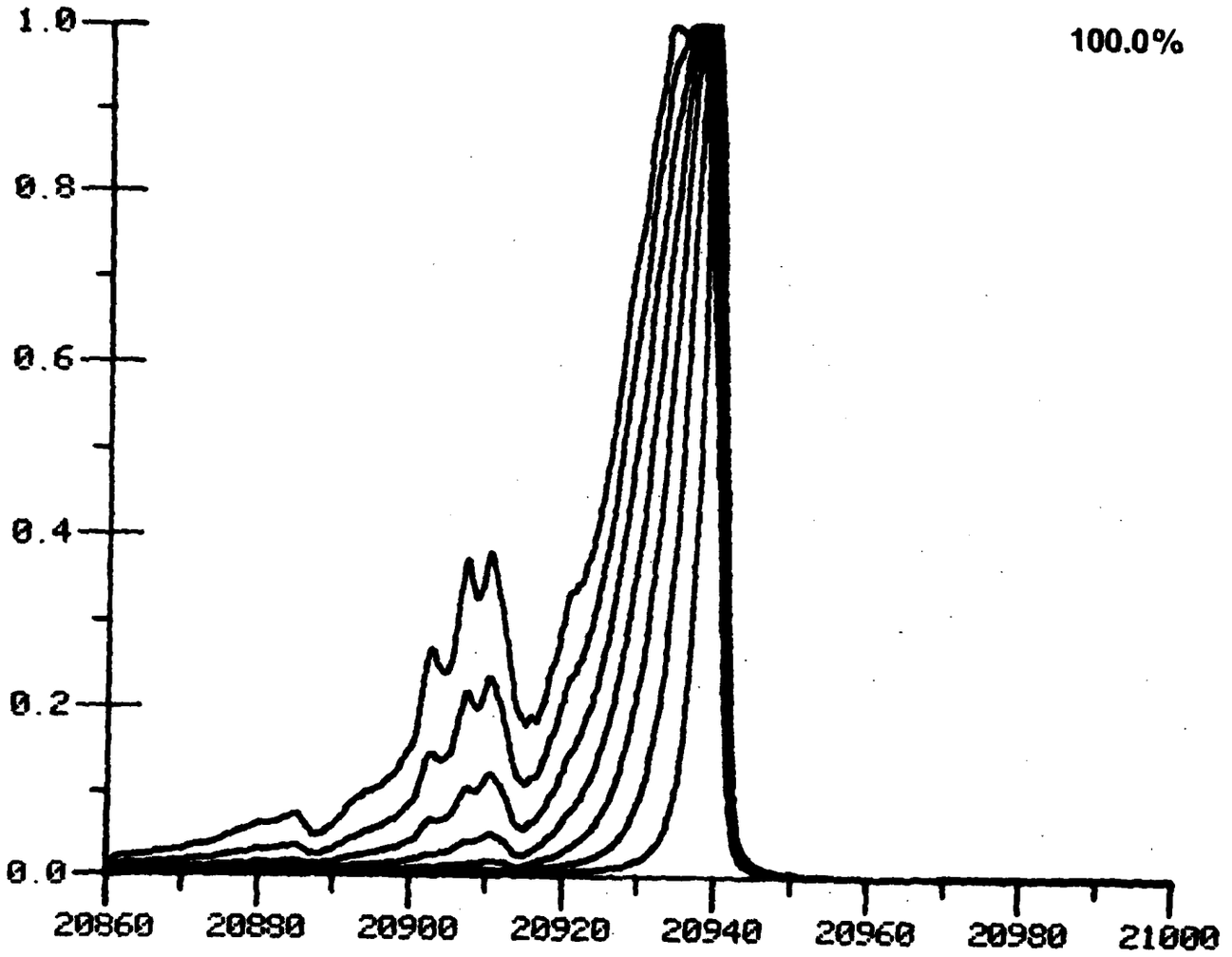
1.0
0.8
0.6
0.4
0.2
0.0
100.0%
20860
20880
20900
20920
20940
20960
20980
21000

Temperature Series

The following graphs present the CO concentration behavior of CARS spectra at a fixed temperature over the range of temperatures from $300^{o}K$ to $2100^{o}K$ in 300 K increments. The concentration values employed in the calculations vary from top to bottom in each graph and are respectively, 0.5, 1.0, 2.0, 5.0, 10.0, 20.0 and 100.0% respectively.

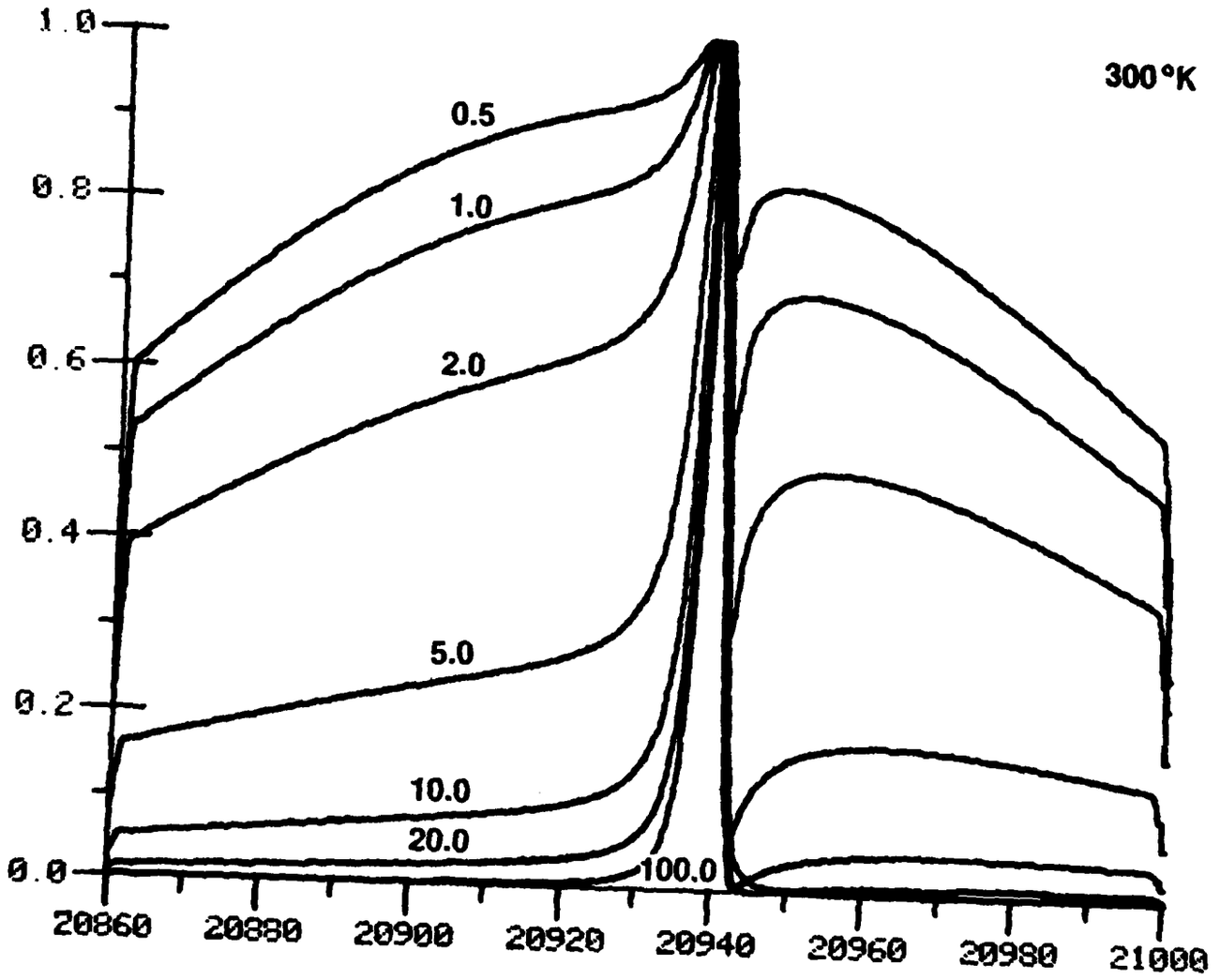
300°K
1.0
0.8
0.6
0.4
0.2
0.0
0.5
1.0
2.0
5.0
10.0
20.0
100.0
20860
20880
20900
20920
20940
20960
20980
21000

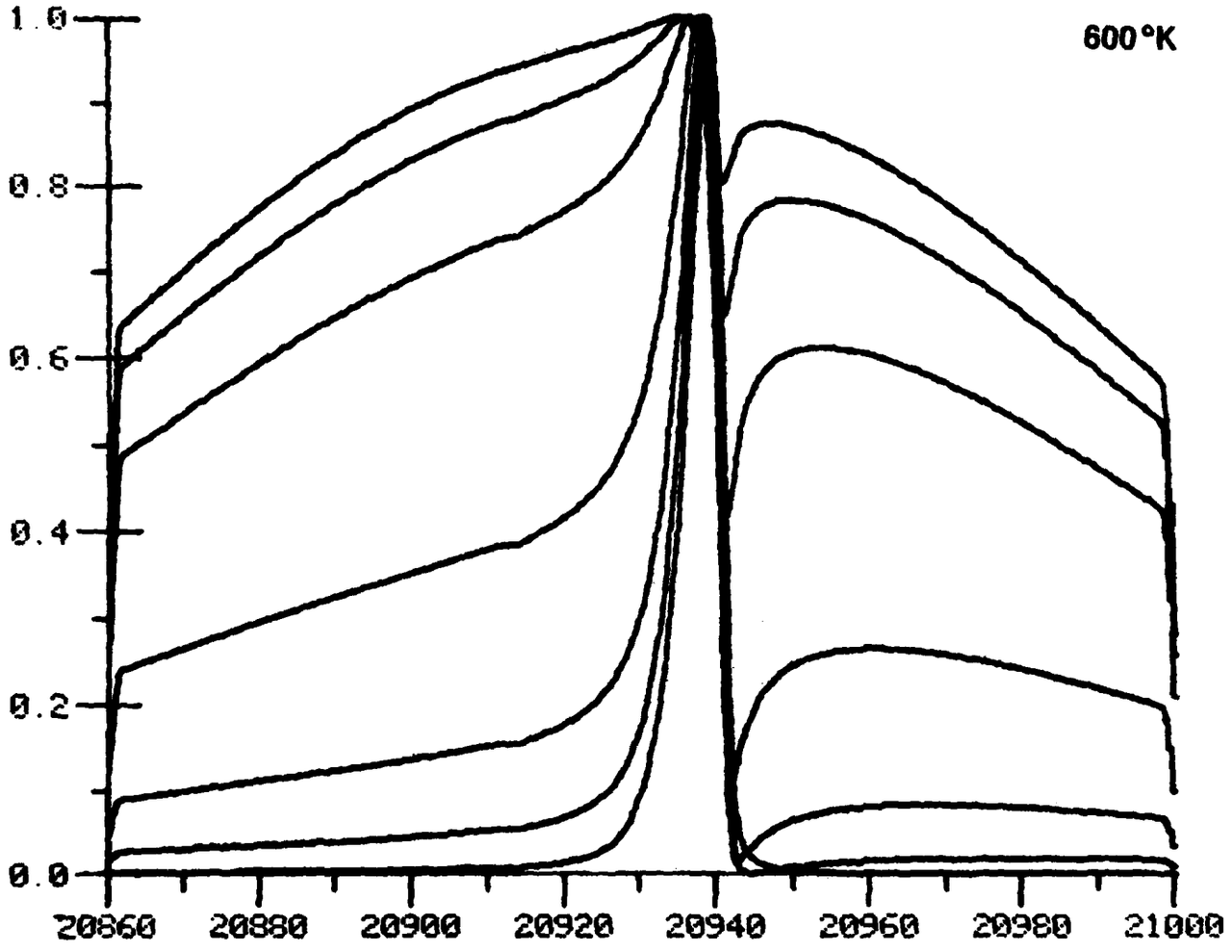
600°K
1.0
0.8
0.6
0.4
0.2
0.0
20860
20880
20900
20920
20940
20960
20980
21000

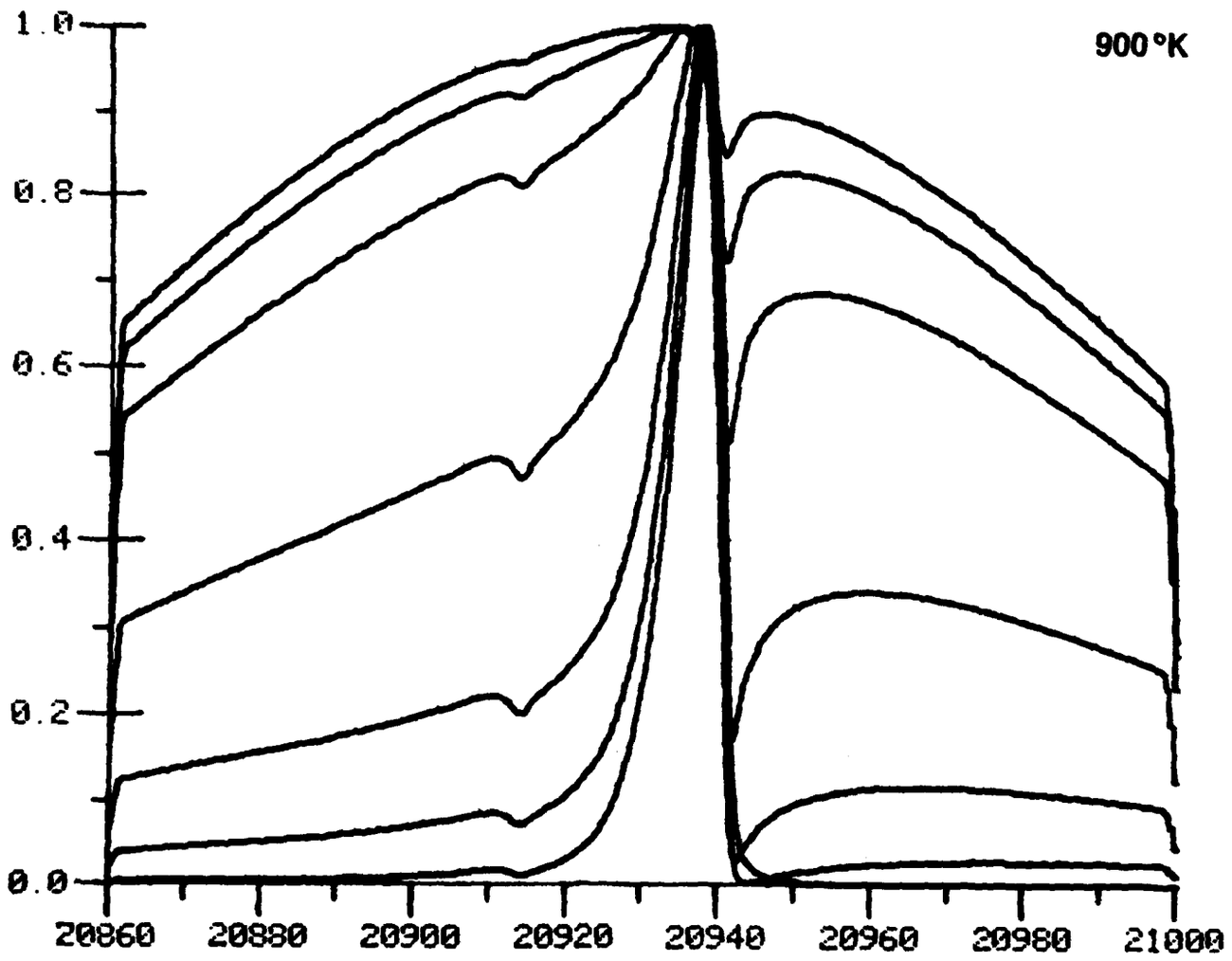
900°K
1.0
0.8
0.6
0.4
0.2
0.0
20860
20880
20900
20920
20940
20960
20980
21000

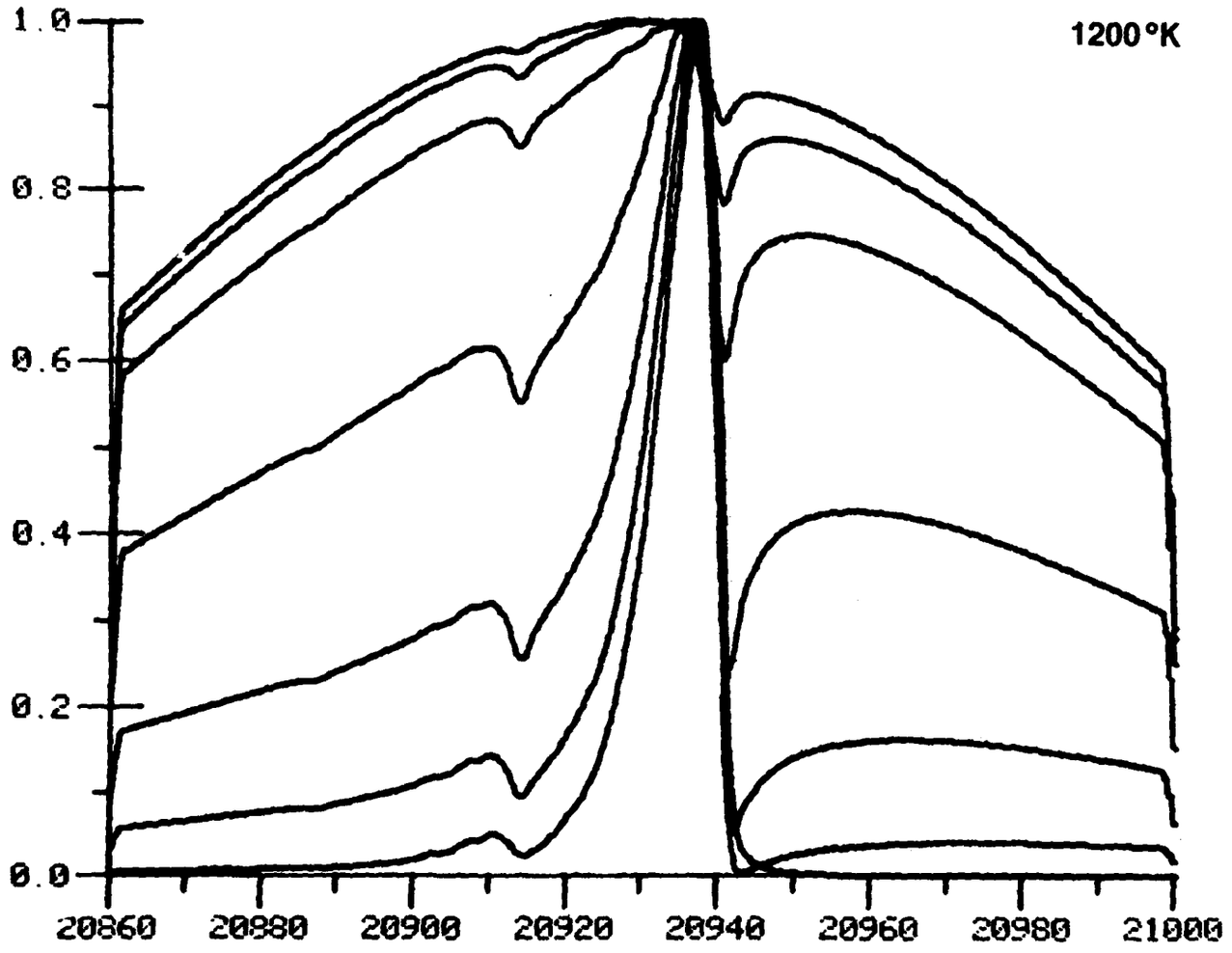
1200°K
1.0
0.8
0.6
0.4
0.2
0.0
20860
20880
20900
20920
20940
20960
20980
21000

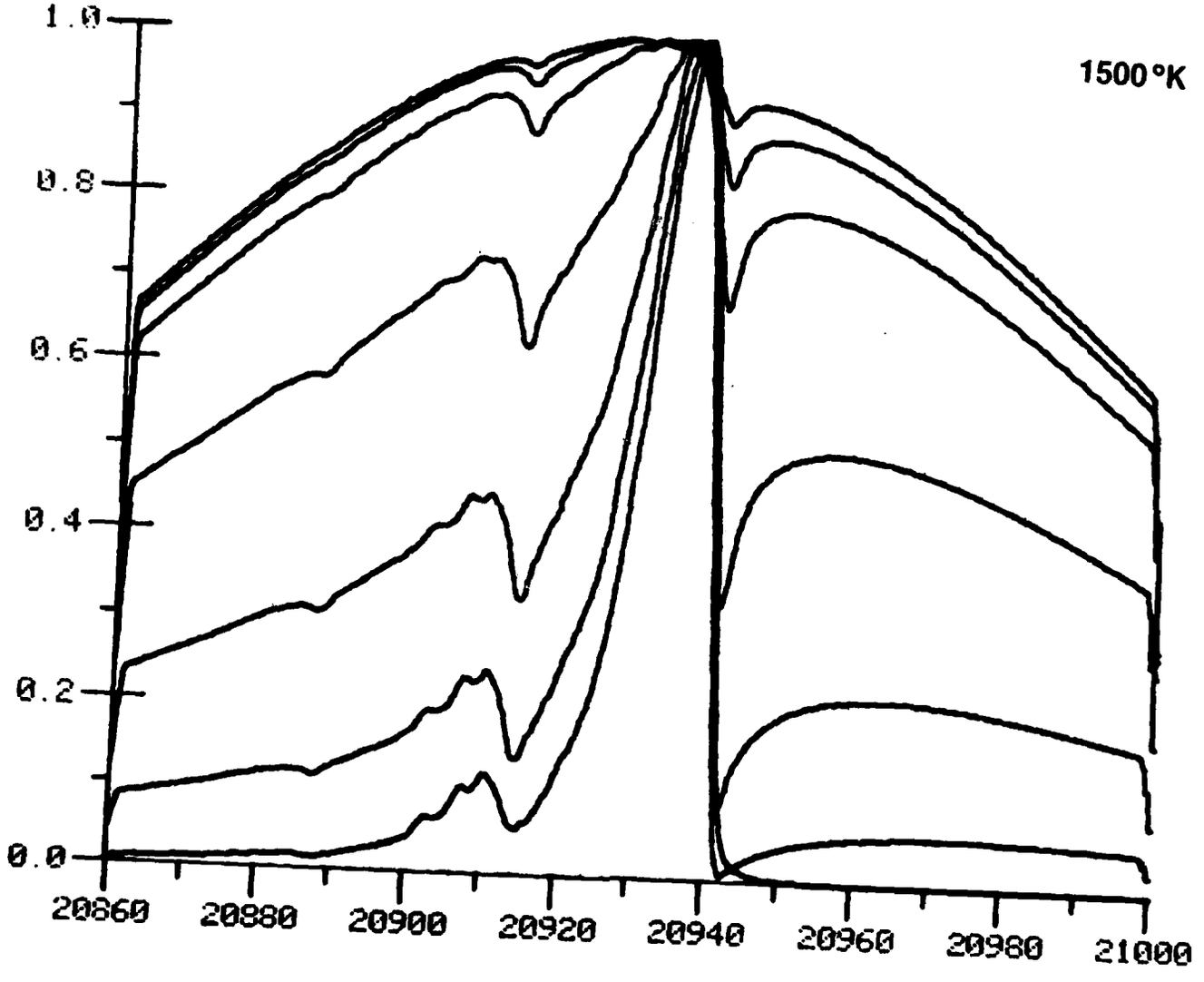
1500°K
1.0
0.8
0.6
0.4
0.2
0.0
20860
20880
20900
20920
20940
20960
20980
21000

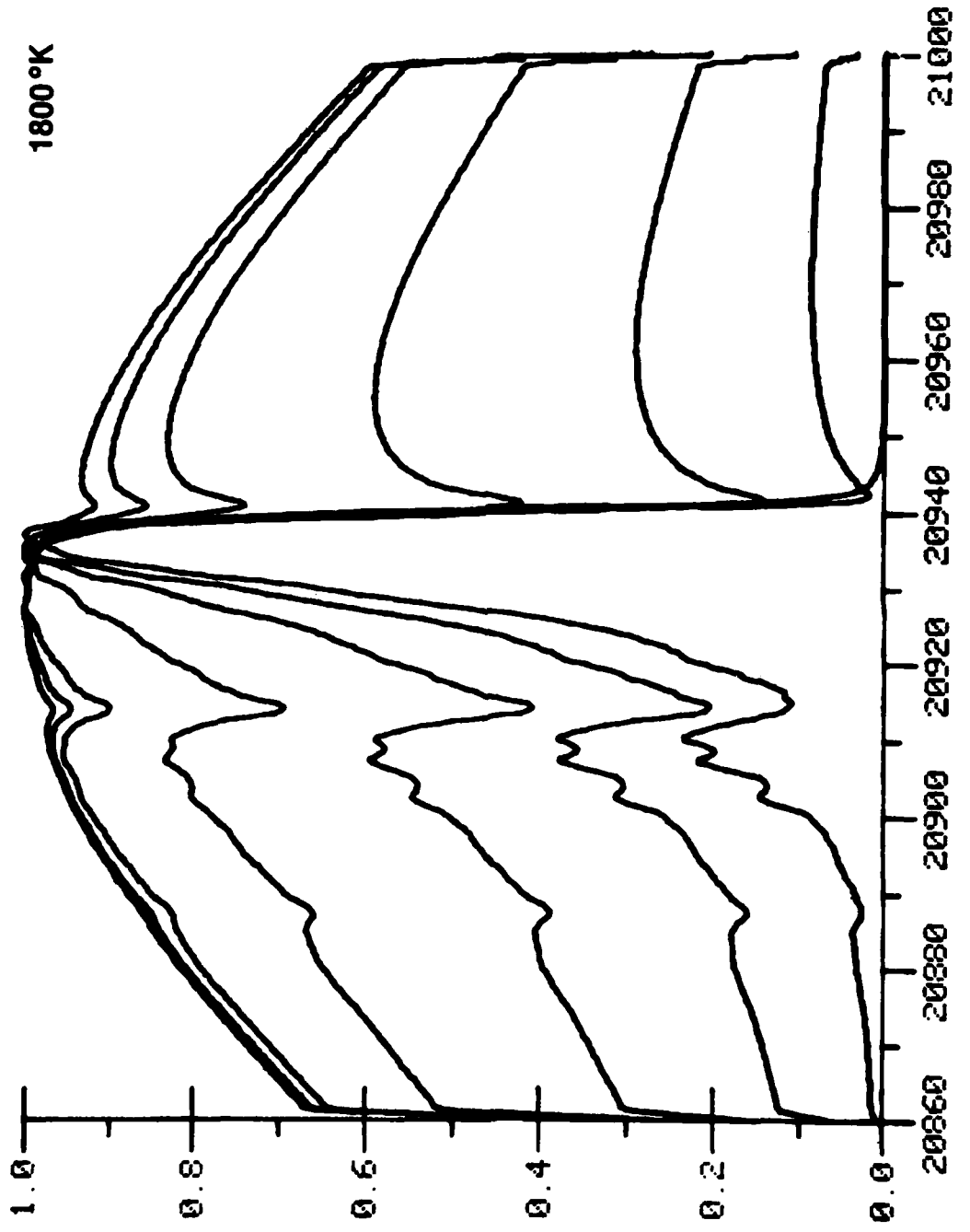
1800°K
1.0
0.8
0.6
0.4
0.2
0.0
20860
20880
20900
20920
20940
20960
20980
21000

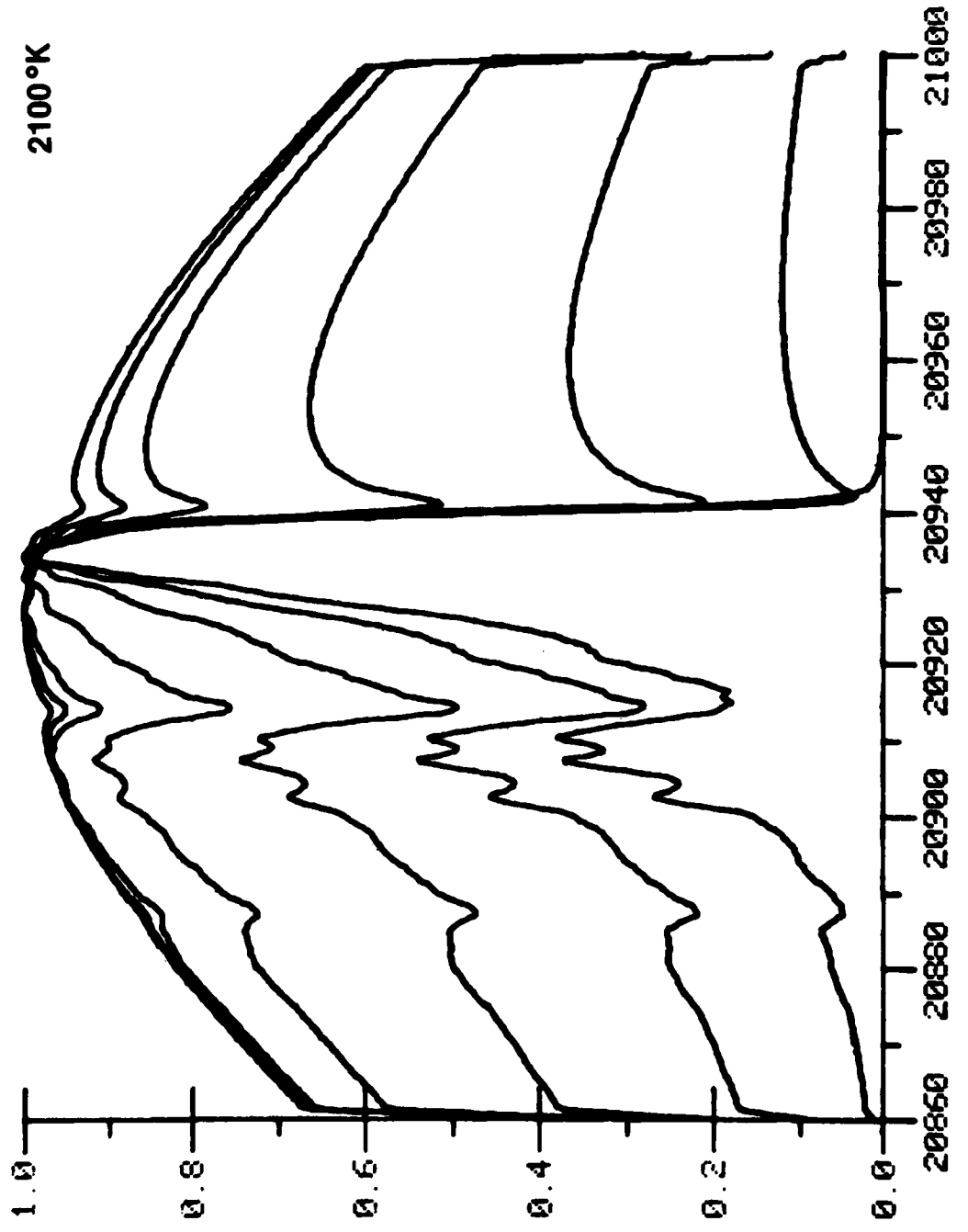
2100°K
1.0
0.8
0.6
0.4
0.2
0.0
20860
20880
20900
20920
20940
20960
20980
21000